

Master Thesis - M.Sc. Electrical Engineering

GUI for System Dimensioning and QO Channel Analysis of Pulsed Pico-second Radar

Saurabh Sanjayrao Nerkar 5045274

August 25, 2021

GUI for System Dimensioning and QO Channel Analysis of Pulsed Pico-second Radar (August 25, 2021)

Copyright © 2021 Saurabh Sanjayrao Nerkar

All rights reserved.



Preface

In this work, a Matlab Graphical User Interface (GUI) tool is built. The two primary goals of the tool are to dimension and design a pulsed pico-second radar which utilizes Photoconductive antennas (PCAs) at the transmitter and to analyze the Quasi-optical (QO) channel of the radar. The mentioned radar is a Terahertz (THz) time-domain system and it is proposed to attain high-resolution real-time security imaging, which is not attainable with the currently available microwave radars. The tool is divided into three parts, the first part of the tool is called as the Transmitter interface, it quantifies the power radiated by a user defined photoconductive antenna array with a user defined pico-second laser at the input of the array. Norton equivalent circuit of the PCA is implemented in this tool to perform this quantification. Apart from the analysis of the radiated power, the tool is can be used to analyze the PCA in detail i.e. it can provide insights in the conductance of the PCA semiconductor gap, the current flowing across the semiconductor gap, and the energy spectrum of the PCA. The second part of the tool is called as the QO Channel Analyzer interface. This part analyzes the Quasi-optical (QO) channel of the radar and quantifies various system efficiencies such as the spillover efficiency of the system, the front-to-back efficiency of the PCA, the detection efficiency of the system and the spillover efficiency of the hemispherical lens. Together these efficiencies characterize the THz power loss in the QO channel. Analysis of these efficiencies is crucial in design and development of the radar. This part of the tool combines the PCA simulations in the CST with the QO system simulation in the TICRA GRASP and PO simulations in Matlab. It automates these simulations to reduce the human efforts. The third part of the tool is referred to as the Main interface. This part analyzes the radar parameters such as the integration time, acquisition time, field of view and resolution of the radar and designs the radar on the system level. The Matlab tool was used to analyze a Bow-tie antenna as a PCA.

This thesis is submitted in partial fulfillment of the requirements for the degree of Master of Science in Electrical Engineering at Delft University of Technology.

Saurabh Sanjayrao Nerkar

Delft, August 2021

Acknowledgments

First of all, I would like to express my gratitude to prof. dr. Andrea Neto for giving me this wonderful opportunity of working on my thesis at TeraHertz Sensing group. You were an inspiration and I was fascinated and attracted towards your passion for and expertise in the field of Electromagnetism since the first quarter of studies at the university. Over the period of my masters I have learned a lot from you. I would also like to thank you for patiently guiding me during my thesis project. You were a great supervisor, thank you for patiently listening to my questions and helping me out.

I would sincerely like to thank Huasheng Zhang, my daily supervisor. In a nutshell, I can say that I would not have been able to complete this project without your help. I cannot thank you enough for the amount of time you have spent on instructing me and solving my doubts. Thank you for patiently listening to my numerous questions and helping me out at every point I was stuck with an obstacle. I appreciate the time and effort you have spent in supervising me throughout the last year.

I would like to thank each and everyone in the TeraHertz sensing group. It was great interacting with such brilliant minds. Thank you for accommodating and helping me time to time. I would also like to thank prof. dr. Nuria Llombart and dr. F. Fioranelli for being a part of my thesis committee.

Furthermore, I would like to thank my dear friends in the Netherlands, specially Parth, Himani and Shaurya for making the life here comfortable and happy. I would also like to thank all my dear friends back in India, specially Rushikesh and Devidas, for encouraging and supporting me throughout my journey.

I would also like to thank each and everyone for supporting me throughout my hard times. It was not an easy journey after my mother passed away. However, all of you accommodated, understood and supported me. I cannot thank you enough for that kind of compassion and support.

Before the end, I would like to express my most sincere gratitude to my family. Without my parents and brother, this whole journey would not have been possible. It is impossible to thank you for the sacrifices you made for me. Words are not enough, we went through the toughest of times but you did not lose hope and taught me to go beyond my limits. I love you!

Finally, I would like to thank Sri Krishna, my dearest friend and the one who sustains the multiverse. Your words gave the strength and the courage to face the impossible and reach the end goals. With Krishna's blessings, I dedicate my thesis to Aai, my mother. Aai, hope you are in bliss. I miss you, and I love you!

GUI for System Dimensioning and QO Channel Analysis of Pulsed Pico-second Radar

This thesis is submitted in partial fulfillment of the requirements for the degree of

MASTER OF SCIENCE

in

ELECTRICAL ENGINEERING

by

Saurabh Sanjayrao Nerkar

born in Beed, India

The work presented in this thesis was performed at:

Tera-Hertz Sensing Group

Department of Microelectronics

Faculty of Electrical Engineering, Mathematics and Computer Science

Delft University of Technology



DELFT UNIVERSITY OF TECHNOLOGY
DEPARTMENT OF ELECTRICAL ENGINEERING

The undersigned hereby certify that they have read and recommend to the Faculty of Electrical Engineering, Mathematics and Computer Science for acceptance a thesis entitled “ **GUI for System Dimensioning and QO Channel Analysis of Pulsed Pico-second Radar** ” by **Saurabh Sanjayrao Nerkar** in partial fulfillment of the requirements for the degree of **Master of Science**.

Dated: August 25, 2021

Chairman:

prof. dr. Andrea Neto

Advisor:

dr. Nuria Llombart Juan

Committee Members:

dr. Francesco Fioranelli

Huasheng Zhang

Contents

Preface	i
Acknowledgments	iii
List of Figures	xi
1 Introduction	1
1.1 Sub-mm Security Imaging and PCA	1
1.2 Radar Scenario and the Matlab Tool	3
1.3 Thesis Outline	4
2 Circuit Model and Detected Power of the PCAs	5
2.1 Norton Equivalent Circuit Model of the PCA	6
2.1.1 Time-domain Analysis	8
2.1.2 Frequency-domain Analysis	10
2.2 Estimation of Detected Power - QO Channel Model	12
2.2.1 Analysis of the Lens Antenna	15
2.2.2 Analysis of the QO Path	17
3 The Matlab GUI Tool	21
3.1 Transmitter Interface	21
3.1.1 Input: Dimensions of the Gap and the connected array of PCAs	23
3.1.2 Input: Laser Details	23
3.1.3 Input: Material Properties and Bias voltage	24
3.1.4 Outputs	26
3.2 QO Channel Analyzer Interface	30
3.2.1 Frequency Sampling	31
3.2.2 PO Simulation	32
3.2.3 GRASP Simulation	36

3.2.4	Outputs	39
3.3	Main Interface	40
3.3.1	Theoretical background	40
3.3.2	Input: Power Radiated by Tx	44
3.3.3	Input: Frequency of Operation and FPA Details	45
3.3.4	Input: QO Channel and Rx Inputs	47
3.3.5	Output: QO Channel and Rx Outputs	48
3.3.6	Output: Resolutions and FoV	50
3.3.7	Output: Energy and Power Received per Gap	51
3.3.8	Conclusion	52
4	Conclusion	55
4.1	Summary and Conclusion	55
4.2	Future Work	56
	Bibliography	59
A	Laser Model and Laser GUI	63
A.1	Laser Model	63
A.2	Laser GUI	64
B	Time-Varying Conductance Of Photoconductor Source	67
C	List of Abbreviations	69
D	Nomenclature	71

List of Figures

1.1	PCA based security imaging scenario.	3
1.2	Main interface of the Matlab GUI tool which models the preliminary radar system and estimates the imaging parameters based on estimated power radiated from the transmitter. The transmitter interface and the QO channel analyzer interface can be accessed from this interface.	4
2.1	Norton Equivalent circuit of the PCA, $Z_a(\omega)$ is the antenna impedance in frequency domain. $I_g(\omega)$ is the current generated in the semiconductor gap and $Z_g(\omega)$ is the Norton equivalent impedance of the generator.	7
2.2	(a) PCA schematic representation with the biasing voltage (Inset shows the PCA gap and the co-ordinate system) (b) Photoconductive antenna time-domain circuit representation.	8
2.3	Menlo THz time-domain system. This device is commercially available with inbuilt laser power source.	13
2.4	QO channel model implemented in the Matlab tool. The model consists of a PCA integrated with a hemispherical lens in Tx and two Menlo lenses to focus the transmitted power towards a horn antenna as a receiver.	13
2.5	Ray tracing and QO channel model implemented in TICRA GRASP.	13
2.6	Block diagram that depicts the procedures to evaluate the efficiency terms in the QO model.	14
2.7	Hemispherical lens used in the QO Channel Model along with the ray tracing of EM fields radiated by the lens.	15
2.8	Detector of the QO channel model simulation in GRASP. \vec{E} and \vec{H} fields are calculated on the circular grid (represented by horizontal green markings in the figure) inside the waveguide.	18
3.1	The "Transmitter interface" of the Matlab tool.	22
3.2	Stratification, top view and the semiconductor gap of the Bow-tie antenna used as a PCA to explain the utility of the Matlab tool.	22

3.3	Tx interface input: Dimensions of the semiconductor gap and the connected array of the PCAs	23
3.4	Tx interface input: Laser details.	23
3.5	Tx interface input: PCA semiconductor gap material properties and bias voltage applied to the PCA unit cell in the PCA array.	25
3.6	Tx interface output: the section of the Tx interface that provides access to the outputs obtained.	26
3.7	Power radiated by the PCA as a function of the input average laser power. . . .	28
3.8	Power radiated by the PCA as a function of the bias voltage applied to the PCA.	28
3.9	Energy spectrum of the radiated THz signal for different values of input laser power.	28
3.10	Energy spectrum of the radiated THz signal for different values of the bias voltage applied to the PCA.	28
3.11	Semiconductor gap resistance of the PCA as a function of the input laser power.	29
3.12	Semiconductor gap resistance of the PCA as a function of the bias voltage. . . .	29
3.13	Current induced across the semiconductor gap w.r.t. time for different values of the input laser power.	29
3.14	Current induced across the semiconductor gap w.r.t. time for different values of the bias voltage.	29
3.15	Current induced across the semiconductor gap w.r.t. frequency for different values of the input laser power.	30
3.16	Conductance across the semiconductor gap w.r.t. time for different values of the input laser power.	30
3.17	QO Channel Analyzer interface of the Matlab tool: the inputs and outputs are separated by the dashed boxes, this interface estimates the QO efficiency of the complete channel.	31
3.18	Frequency sampling section of the QO channel interface where the frequencies for which the QO channel model need to be simulated are specified.	31
3.19	PO simulation section of the QO channel interface of the Matlab tool.	32
3.20	The hyperhemispherical lens geometry used with Bow-tie antenna PCA and plotted using the Lens Details interface of the Matlab tool. This geometry does not show the matching layer.	33
3.21	Spillover efficiency of the hemispherical lens estimated by the PO in Tx simulation.	34
3.22	Secondary electric field radiated at 500 GHz by the hemispherical lens estimated by the PO in Tx simulation.	34

3.23	Secondary electric field radiated at 1000 GHz by the hemispherical lens estimated by the PO in Tx simulation.	34
3.24	f2b efficiency calculation section of the QO channel interface.	35
3.25	f2b efficiency of the Bow-tie PCA.	35
3.26	Reflection efficiency, η_{rad}^l of the hemispherical lens.	35
3.27	Lens details interface which takes the lens details as inputs from the user. It can be accessed from the QO channel interface.	36
3.28	GRASP simulation section of the QO channel interface.	37
3.29	Spillover efficiency of the dual Menlo lens system in the QO channel model when the Bow-tie antenna is used as the PCA.	38
3.30	Detection efficiency of the QO channel model receiver when the Bow-tie antenna is used as the PCA.	38
3.31	QO efficiency of the QO channel model when the Bow-tie antenna is used as the PCA.	38
3.32	Interface to update the parameters related to the QO channel model, e.g., the resolution of the GRASP simulation, the distance between the QO-components, etc.	39
3.33	Outputs section of the QO channel interface.	39
3.34	Main interface of the Matlab tool.	40
3.35	Scenario: Spillover calculations	41
3.36	η_{QO} as a function of the distance between the reflector and the target.	42
3.37	Input section of the main interface where the power radiated by the transmitter PCA is specified.	45
3.38	Section of the main interface where frequency of operation of the radar and the FPA details should be provided.	45
3.39	Section of the main interface where the QO channel efficiencies and the desired Rx parameters such as the SNR are specified.	47
3.40	Section of the main interface of the Matlab tool which displays the QO channel and imaging parameters.	49
3.41	Integration time of the radar as a function of the power radiated by the Tx.	49
3.42	Acquisition time of the radar as a function of the power radiated by the Tx.	49
3.43	Detection bandwidth of the radar as a function of the power radiated by the Tx.	50
3.44	Section of the main interface of the Matlab tool that displays the resolution and the FoV of the radar.	50
3.45	FoV of the radar with input parameters as shown in Fig. 3.34.	51

3.46	Section of the main interface that displays the energy and power received at a single PCA gap of the FPA.	51
3.47	Energy received at the gap of a single PCA in the FPA as a function of the power radiated by the Tx.	52
3.48	Power received at the gap of a single PCA in the FPA as a function of the power radiated by the Tx.	52
A.1	Radar GUI: Tx Window: Laser Beam Analysis window	65
A.2	Power spectral density of the laser beam	66
A.3	Spatial distribution of electric field of laser	66

Chapter 1

Introduction

1.1 Sub-mm Security Imaging and PCA

Public safety and security at crowded places or otherwise is a major concern of the government and private entities owning the places around the world. The current security systems viz., CCTV cameras, metal detectors etc. are effective. However, sometimes they fail either because of their inherent dependence on humans or because of advanced weapon technologies that can outmatch these systems. Moreover, for public places such as airports, the imaging systems work mostly at millimeter waves due to the lower cost. However, such devices require a short standoff distance and perform low-resolution imaging, which makes detection more difficult. Installing advanced security systems such as full-body scanners is very expensive and therefore government or private entities across the globe are compelled to use the traditional security systems. This jeopardizes public safety and security and sometimes may lead to the loss of lives.

High-resolution real-time security imaging system at low cost is needed to address the problems in the public safety and security. In last few years, researchers have started exploring the Terahertz (THz) domain to develop such a system considering the wide bandwidth available in THz domain. In [1], a study of standoff detection of weapons and contraband in the region 100 GHz to 1 THz is presented. In this study active imaging, imaging relying on the differences in the reflectivity of the targets, is used to detect a toy gun under the cotton shirt, this active system works at 640 GHz, and passive imaging, imaging based on the temperature difference of the emitted radiated by the object(s), is used to detect a metal knife inside a newspaper.

Moreover, a THz imaging radar operating at 675 GHz was reported by NASA Jet Propulsion Laboratory in [2]. This radar enables fast, reliable and through the cloths imaging that can provide information of the objects, weapons or otherwise that a person is bearing. This study promised a real-time frame rate of 1 Hz. This enables the imaging as soon as the person walks into the radar field. The feature that the imaging is possible as soon as the person walks into the radar field is important as it leads to the possibility of scanning larger crowds in lesser time and

with higher accuracy than the conventional methods. In their study, a person carrying three 1 inch PVC pipes under his cloths was imaged. In the visible spectrum, the pipes are concealed under the cloths however, as soon as the person moves into the radar field the pipes become visible in THz spectrum.

It is evident from [1] and [2] that the THz radars can provide a promising solution to the problems related to public safety and security. However, these radars operate with a bandwidth of the order of a few tens of GHz and can achieve a sub-centimeter resolution only which might make the detection difficult.

To achieve sub-mm resolution bandwidth wider than a few tens of GHz is needed. Recent research in the field of THz time-domain imaging, driven by the photoconductive antennas (PCAs), promises the required larger bandwidth of order of a few hundreds of GHz. Such THz time-domain imaging systems promise sub-mm resolutions and are currently employed for spectroscopy in multiple domains such as chemistry, biology, solid state physics, etc. [3–5]. The PCAs can generate the THz signals with bandwidth up to a few hundreds of GHz at a relatively low cost. [6–15]. However, their limitation is that they can generate the THz power of the order of a few μW only. This limitation makes the THz time-domain systems based on the PCAs unsuitable for the high-resolution security imaging applications. This problem is solved in [16] where a PCA setup is presented which can generate THz power of the order of mW .

Owing to the advantages of the larger bandwidth of the THz time-domain systems and the availability of the PCAs along with the possibility of the generation of THz signals with higher power, the interest of researchers and engineers across the globe in design and development of the THz time-domain radars is growing rapidly. These radars promise high-resolution real-time imaging with the field-of-view (FoV) comparable to the current state-of-the-art sub-mm radars. However, design, development and analysis of such systems is a challenging task. In general, the THz time-domain radar can be divided into three parts: the THz transmitter, the quasi-optical (QO) channel and the receiver of the radar. The main aspect of the transmitter design is that it should produce THz power at least of the order of mW for the radar to work properly. The power loss in the propagation of the THz signal from the transmitter to the receiver of the radar is estimated from the QO path analysis. Finally, principles of detection and imaging are used to estimate the radar parameters such as the received power and energy, the field of view and the resolution of the radar.

Design and analysis of each of the aforementioned parts of the radar system are in itself intense, time-consuming and requires knowledge of multiple subjects. For example, the development of the THz transmitter is driven by the design of PCAs, including the modelling of the optical source, the broadband antenna design, the modelling of the equivalent circuit, and the integration with a lens. These procedures require knowledge of the physics and mathematics that

goes into them. This might not be the area of interest or expertise of a radar designer. A similar argument is true for the QO channel analysis as well. Therefore, the process of designing and analysing a complete THz time-domain radar is a challenging task even for a preliminary design at a top-level. This thesis attempts to solve difficulties in the THz time-domain radar design by introducing a Matlab based Graphical User Interface (GUI), for system dimensioning and QO channel analysis of the radar. The developed Matlab tool allows people to design their desired THz radar system without knowing the fundamentals.

1.2 Radar Scenario and the Matlab Tool

In Fig. 1.1 the application scenario model of the THz time-domain radar being considered for this thesis is visualized.

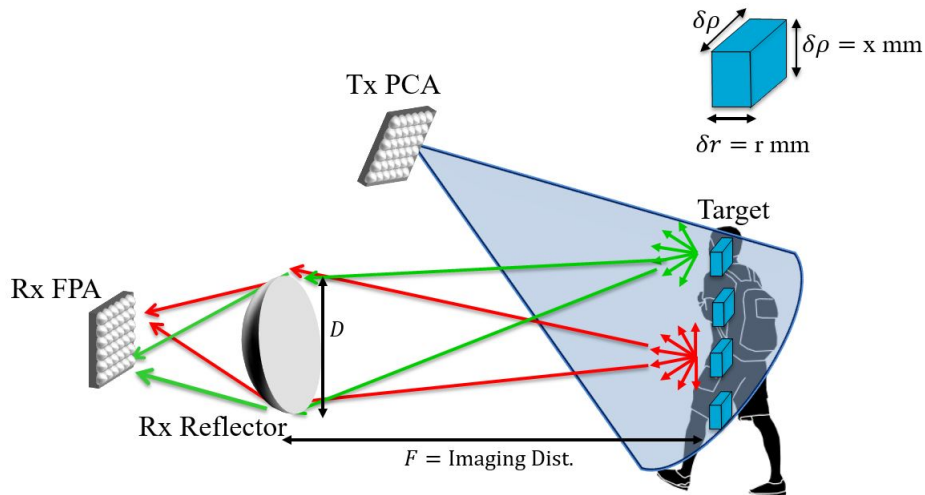


Figure 1.1: PCA based security imaging scenario.

In this scenario, the transmission (Tx) PCA(s) radiate(s) a THz signal, with a minimum power of the order of mW , which is then reflected by the target. The reflected THz signal is focused on to the receiver by utilizing the QO components in the propagation path. For simplicity, we use an on-axis equivalent reflector as the QO component. This power is then received by a focal plane array (FPA) at the receiver. For this specific imaging scenario, the proposed Matlab GUI, shown in Fig. 1.2, will evaluate the preliminary radar parameters, such as the detection bandwidth, the integration and acquisition time, the QO channel efficiency, field of view (FoV), and the resolution of the radar along with the THz power received at the receiver. The Matlab GUI tool is described in detail in Chapter 3, where we will see that the setup in Fig. 1.2 could lead to approximately 4 mm lateral resolution and 1 mm range resolution and the FoV can be around $6\text{ cm} \times 6\text{ cm} \times 100\text{ cm}$ at 1 Hz imaging speed provided the power radiated is 1 mW and the frequency of operation of the transmitter is $100\text{ GHz} - 400\text{ GHz}$.

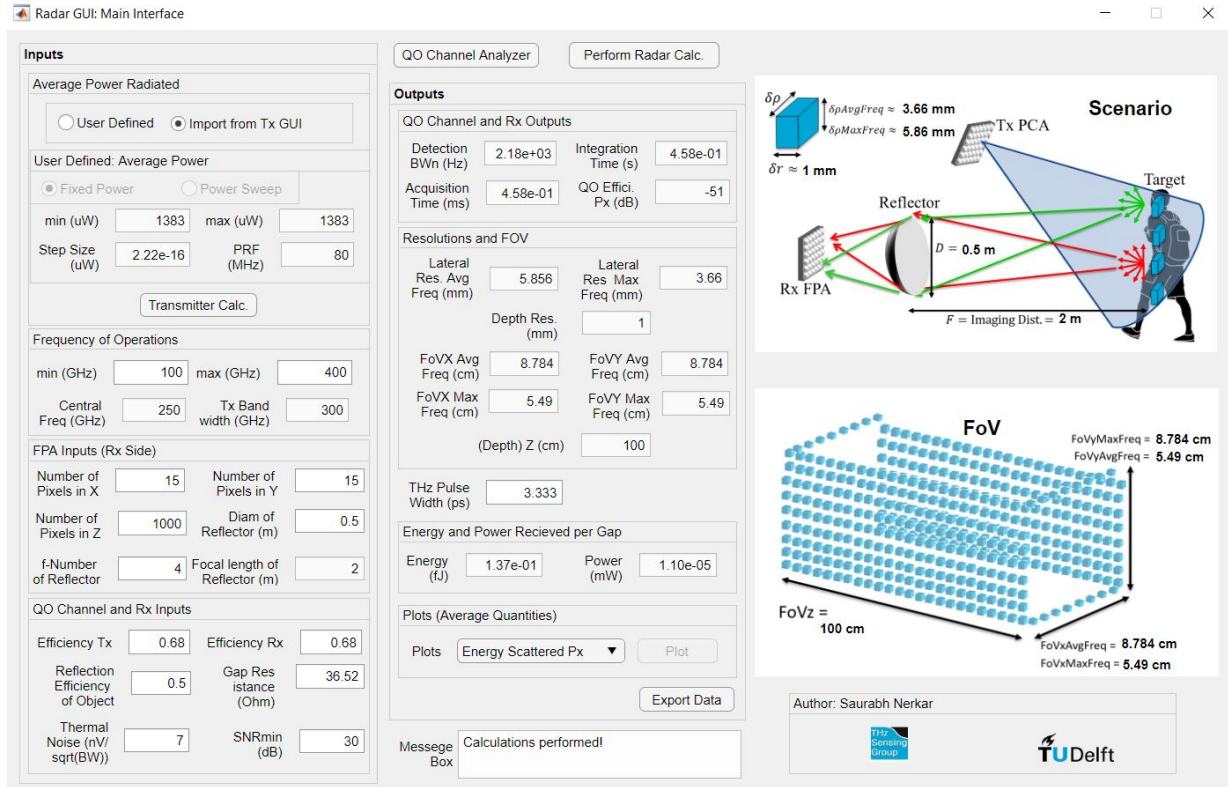


Figure 1.2: Main interface of the Matlab GUI tool which models the preliminary radar system and estimates the imaging parameters based on estimated power radiated from the transmitter. The transmitter interface and the QO channel analyzer interface can be accessed from this interface.

1.3 Thesis Outline

The thesis structure is discussed in this section. This thesis consists of four chapters. Chapter 2 describes the circuit model of the PCA and the QO channel model implemented in the thesis along with the theoretical background of these models. The circuit model of the PCA quantifies the power radiated by the transmitter PCA and the QO channel model estimates the power loss in the channel and evaluates the power detected at the receiver.

Chapter 3 describes the three interfaces of the Matlab GUI tool namely, the "Main interface", the "Transmitter interface" and the "QO Channel Analyzer interface" along with their supplementary interfaces. The theory behind the estimation of the imaging parameters is described in the relevant sections. The chapter explains the interfaces with an example of the Bow-tie antenna as a PCA and the results obtained from the tool for the Bow-tie PCA are also presented in this chapter.

Finally, chapter 4 concludes the thesis and discusses the future work related to the developed Matlab GUI tool.

Chapter 2

Circuit Model and Detected Power of the PCAs

In the previous chapter, it is mentioned that the design and development of the THz time-domain radar is a challenging and time-consuming task. Different aspects of the design require a deep understanding of background knowledge of different domains. The design and development of the THz radar transmitter require a background knowledge of the physics and the mathematics behind the PCAs. The propagation of the emitted THz signals among different objects should be analyzed using the QO principles. Moreover, the specifications involved in the radar receiver require the knowledge of detection and imaging. This thesis proposes a Matlab GUI that provides a one-stop solution to simplify the three-part system design process of the THz time-domain radar. The tool serves multiple purposes in THz radar design: it analyzes the power radiated by an existing PCA, couples the existing PCAs to lenses, analyzes a pre-defined QO channel that reflects the radar scenario, and estimates the radar imaging parameters for the inputs given by the user. Although the whole analysis of the tool is automated and pre-defined, users with more background knowledge would benefit more, since there are various inputs that can be tuned to achieve a desired goal. This chapter deals with the theoretical background of the models implemented in the thesis and the details of the tunable input parameters in the Matlab tool will be described in chapter 3.

As mentioned before, the radar scenario, shown in Fig. 1.1, is divided into three parts, namely PCA in Tx, QO channel analysis, and the PCA in Rx. In this chapter we mainly focus on the first two aspects. The PCA in Tx was modelled by a Norton equivalent circuit [17] to quantify the radiated THz power and other parameters of the PCA. The QO channel between the transmitter and the receiver was modelled by a commercial Menlo system.

In this chapter, the aforementioned theoretical models behind the tool are introduced along with the mathematical underpinning of the calculations performed by the tool in relation to

these theoretical models. Understanding the theoretical models and the mathematics involved is important in order to validate the accuracy of the results, understand the basis of the results, and understand the limiting conditions of the tool in real world application scenario. Familiarity with the input and output parameters and their calculations in the theoretical models help in understanding the use cases and the usage of the tool. Familiarity with the theoretical background is also helpful to navigate the interface of the tool described in detail in chapter 3.

2.1 Norton Equivalent Circuit Model of the PCA

In the literature, we have known that the PCAs are the low-cost means of THz signal generation [6–15]. Therefore, they drive variety of modern-day THz applications, including THz radars. PCAs are the backbone of a THz radar as they are used to generate the THz signals. PCAs generate the THz signals when impinged on by an optical source. They are made of a metallization printed over a semiconductor, biased by an external voltage source and pumped by the lasers to generate the THz power. A laser with a specific carrier frequency impinges on the semiconductor material and provides sufficient energy to the electrons inside the semiconductor to move from the valence band to the conduction band. This generates free electron-hole pairs, the presence of which produces a change of the conductivity of the material and the material becomes a photoconductor. Two important factors which are responsible for the change in the conductivity of the semiconductor material are the operational mode of lasers i.e. continuous wave (CW) [9] or pulsed wave (PW) [6] and the lifetime of the carriers in the material. In presence of a biasing voltage, inducing an electric field across the semiconductor gap by the laser (in transmission) or impinging it with THz radiation (in reception), aforementioned free charges are accelerated. Accelerated free charges induce a time-varying current across the semiconductor gap of the PCA. This effect causes propagation of an electric field in the surrounding antenna structure. Modulating signal of the laser pump and the semiconductor response to the laser excitation along with the geometrical structure of the antenna affects the frequency of the propagating signal mentioned previously [18].

The limitation of a single PCA unit is that the power available for transmission is in the order of μW which is limited by multiple factors, such as the number of charges that can be excited to the conduction band in the material, the mean velocity of the charge carriers, the coupling between the photoconductor gap and the surrounding antenna structure and the thermal failure of the device [6, 7]. This power may turn out to be sufficient for spectroscopy applications in the field of molecular biology or chemistry. However, it is not sufficient for applications such as high-resolution security imaging. A solution to this problem is stated in [16] and [18], these research works propose a connected array of the PCAs to generate THz signal with power of the order of $1 mW$.

In essence, designing and developing THz time-domain transmitters for different applications comes down to modelling, designing and analyzing PCAs. Multiple researchers have contributed state-of-the-art research in this field [9, 10, 13, 15, 19]. In [20] a simple but effective Norton equivalent circuit of PCAs for PW operating mode of lasers is described. This model takes into account, optical, electrical and geometrical parameters of photoconductive generator. The Norton circuit models the coupling between the semiconductor gap and the antenna surrounding it. This aspect of the model makes it extremely useful to quantify the the power radiated by an antenna. Figure 2.1 shows the frequency-domain Norton equivalent circuit of the PCA. In [21], this circuit model was validated by a measurement based on a dual-reflector system. Therefore, in this thesis we can resort to this model to perform. Theoretical background of the Norton circuit of a PCA is understood by performing time-domain and frequency-domain analysis on it which will be discussed explicitly in the following subsection.

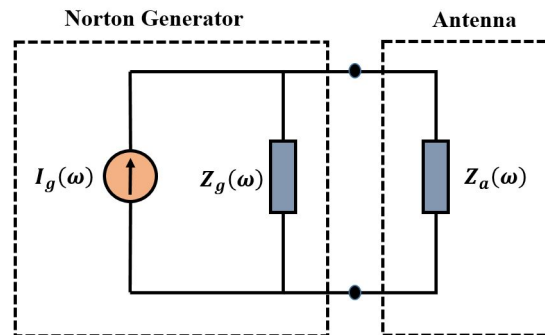


Figure 2.1: Norton Equivalent circuit of the PCA, $Z_a(\omega)$ is the antenna impedance in frequency domain. $I_g(\omega)$ is the current generated in the semiconductor gap and $Z_g(\omega)$ is the Norton equivalent impedance of the generator.

The maximum power radiated by the PCA is limited by the biasing voltage applied to the semiconductor gap. The biasing voltage can not exceed the value of breakdown voltage of the semiconductor material of the PCAs, which is usually low-temperature Gallium rsenide (LT-GaAs). A biasing voltage higher than the breakdown voltage could lead to thermal failure of the device. This phenomena drastically reduces the possibility of using the PCAs and in turn the THz time-domain systems in applications that require higher power for operation i.e. radar applications. To solve this issue, research described in [16] discusses an implementation of the connected arrays of the PCAs. In [16], a pulsed photoconductive terahertz source is presented that can produce THz power of the order of mW and can utilize the ultra-wideband characteristics of the connected arrays.

It has been seen so far that the Norton circuit model of the PCAs is a fairly accurate and extremely helpful in quantifying the radiated power of a PCA. Apart from radiated power, the model gives insights into multiple other quantities that are important for understanding the behaviour of the PCAs viz., the conductance of the PCA, the energy spectrum, the current

across the semiconductor gap etc. The model is analytical in nature and performs better in comparison with other PCA models [20]. Considering [16] and [18] it is safe to assume that THz powers sufficient for the radar applications are possible. Therefore, the Norton equivalent circuit model of the PCAs is implemented in the Matlab tool. Furthermore, the tool is able to analyze the Norton circuit model parametrically over input laser power to the PCA and the input bias voltage of the PCA. A limitation of the model implemented in the tool is that the power output of the PCA array is calculated linearly instead of implementing the connected arrays of the PCAs.

Table 2.1 summarizes the input and output parameters of the Norton circuit model of the PCAs implemented in the tool.

Until this point, the Norton circuit model of the PCA implemented in this thesis work was discussed in brief. The subsequent subsections discuss the theoretical background of the Norton circuit through performing time-domain and frequency-domain analysis of the circuit.

2.1.1 Time-domain Analysis

Let's consider a scenario described in Fig. 2.2 [20]. Fig. 2.2a, represents a schematic of the photoconductor antenna with a biasing network. The inset in the figure showcases the coordinate system utilized for the analysis and the semiconductor gap of the PCA.

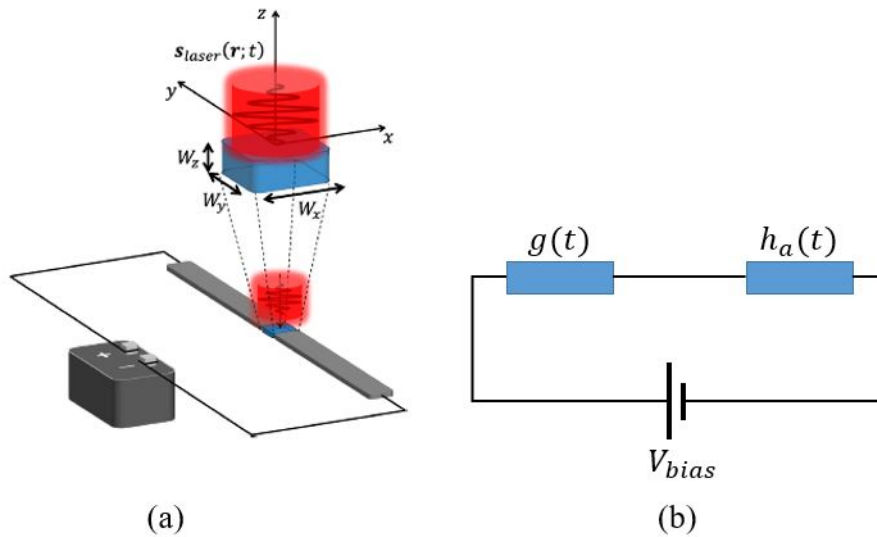


Figure 2.2: (a) PCA schematic representation with the biasing voltage (Inset shows the PCA gap and the coordinate system) (b) Photoconductive antenna time-domain circuit representation.

It can be seen in Fig. 2.2 that the laser beam characterized by an average power density of $s_{laser}(\mathbf{r}; t)$ impinges on the semiconductor gap. Fig. 2.2b, represents the photoconductive antenna time-domain circuit. V_{bias} is the external bias voltage applied to the antenna, $g(t)$ is the time-varying conductance induced in the semiconductor gap due to the impinging laser beam

and $h_a(t)$ is the impulse response of the semiconductor material to the laser excitation. W_x , W_y and W_z are the width, length and height of the of the semiconductor gap respectively.

While dealing with the Norton equivalent circuit of the PCA it has to be noted that, the photoconductive gap dimensions of the antenna are assumed to be small with respect to the wavelength of the highest frequency of the pulse bandwidth in PW mode. It is also assumed that the semiconductor gap gets uniform illumination from the laser beam. In order to achieve uniform illumination, it is assumed that the laser spot is comparable or bigger than the semiconductor gap size. The electric field and current generated in the semiconductor gap of the PCAs by an impinging laser are assumed to be uniform and independent of z .

Power spectral density of the laser beam denoted by $s_{laser}(\mathbf{r};t)$ is explicitly defined in Appendix A. The time-varying conductance of the semiconductor gap induced by the laser field can then be calculated as follows:

$$g(t) = \eta(W_x, W_y, W_z, A_{laser}) \frac{A_{laser}}{W_y^2} e\mu h(t) \otimes \tilde{s}(t) \quad (2.1)$$

where, η is defined to be the laser power absorption efficiency of the photoconductor gap, this quantity takes into account different factors viz., spillover of the laser beam with respect to the photoconductor gap size, the reflection at the air-photoconductor interface and the laser power absorption property of the photoconductor (symbolically represented as α). The term $\tilde{s}(t)$ is the time-varying envelope of the laser pulse. The term A_{laser} in Eq. (2.1) is known as the effective area of the impinging laser beam and it is defined in Appendix A. Finally, the term $h(t)$ is the impulse response of the semiconductor gap with respect to the laser excitation, it is given as,

$$h(t) = \frac{1}{hf_g} e^{-\frac{t}{\tau}} u(t) \quad (2.2)$$

where, e is the charge of an electron and μ is the mobility of the charge carriers in the semiconductor material, it is given by Eq. (B.8) described in the Appendix B. Appendix B sheds more light on the derivation of the time-varying conductance of the semiconductor gap.

The current flowing across the semiconductor gap is calculated using the relation below:

$$i_g(t) = g(t)V_{bias} \quad (2.3)$$

where, V_{bias} is the biasing voltage applied to the PCA semiconductor gap as mentioned before.

By assuming a uniformly distributed electric field, the total electric field across the semiconductor gap is obtained as follows:

$$e(r;t) = -\frac{V_{bias}}{W_y} \hat{y} \quad (2.4)$$

2.1.2 Frequency-domain Analysis

It is established that the coupling between the antenna and the semiconductor gap can be well understood if a Norton equivalent circuit of the PCA is used [20]. Norton's theorem states that in frequency domain, the current flowing in a load across the terminals of a complex linear electrical system can be obtained by replacing the entire circuit with just two components i.e. an equivalent current generator and an equivalent impedance. This will provide a representation of the complex circuit completely decoupled [20].

Fig. 2.1 represents the frequency-domain Norton circuit equivalent of the PCA, where, $I_g(\omega)$ is the equivalent generator current flowing across the semiconductor gap and $Z_g(\omega)$ is equivalent generator impedance i.e. impedance of the semiconductor gap of the PCA. $Z_a(\omega)$ is the frequency domain impedance of the load i.e. antenna.

The current $I_g(\omega)$ is the Fourier transform of the current across the semiconductor gap given by the Eq. (2.3), $I_g(\omega) = FT[i_g(t)]$. The current $I_g(\omega)$ can be obtained by using the expression given below:

$$I_g(\omega) = \eta(W_x, W_y, W_z, A_{laser}) \frac{A_{laser}}{W_y^2} e\mu H(\omega) \tilde{S}(\omega) V_{bias} \quad (2.5)$$

where, $\tilde{S}(\omega)$ is the Fourier transform of the average power density of the laser source, $H(\omega)$ is the Fourier transform of the impulse response of the semiconductor gap to the laser excitation, it is given as,

$$FT[h(t)] = H(\omega) = \frac{1}{hf_g} \frac{\tau_c}{1 + j\tau_c\omega} \quad (2.6)$$

where, h is the Planck's constant, f_g is the frequency of the semiconductor gap which corresponds to the energy required to excite an electron from valence band to the conduction band of the semiconductor gap. τ_c is the charge combination time of the semiconductor gap of the PCA.

Norton equivalent generator impedance is given as below:

$$Z_g(\omega) = \frac{V(\omega)}{I_g(\omega)} \quad (2.7)$$

However, Eq. (2.7) is difficult to implement. Therefore, Norton equivalent generator impedance is approximated to a constant impedance over the semiconductor gap, this constant impedance is known as R_g and it is given as below:

$$R_{gap} = \frac{2W_x^2}{\mu_{dc}\eta_{opt}\tilde{P}_{laser}\left[qe\frac{T}{hf_c}\right]} \frac{(\tau_c + \tau_s)}{(\tau_c - \tau_s)} \quad (2.8)$$

where, q_e is the charge of an electron, T is the Pulse Repetition Time (PRT) of the laser signal, f_c is the laser carrier frequency, and τ_s is the scattering time of the charge carriers in the semiconductor material.

Once the current and voltage of the PCA are known, its energy spectral density can be evaluated as:

$$E_s = V_a(\omega) * I_a^*(\omega) = Z_a(\omega) \left| \frac{Z_g(\omega)}{Z_a(\omega) + Z_g(\omega)} \right|^2 |I_g(\omega)|^2 \quad (2.9)$$

By substituting Eq. (2.8) in Eq. (2.9):

$$E_s = Z_a \left| \frac{R_{gap}}{Z_a + R_{gap}} \right|^2 |I_g(\omega)|^2 \quad (2.10)$$

And then the radiated energy can be obtained as an integration of the spectrum:

$$E_{rad} = \frac{1}{2\pi} \int_{-\infty}^{+\infty} E_s(\omega) d\omega \quad (2.11)$$

Then, the power radiated by the PCA can be expressed as:

$$\tilde{P}_{rad} = \frac{E_{rad}}{T} \quad (2.12)$$

There is always going to be an impedance mismatch between the antenna impedance and the impedance of the semiconductor gap, giving rise to the loss of power. This power loss is quantified by a term matching efficiency. Matching efficiency between antenna and photoconductive source, denoted by η_m , is defined as the ratio between the energy radiated by the antenna and the maximum energy available at the photoconductive source. Matching efficiency is expressed as follows:

$$\eta_m(\omega) = \frac{E_s(\omega)}{E_s^{max}(\omega)} \quad (2.13)$$

where, $E_s(\omega)$ is the energy spectrum and $E_s^{max}(\omega)$ is the maximum possible value of the energy spectrum of antenna radiation.

From the definition of the matching efficiency it can be understood that although the power radiated by the PCA is given using (2.12), the power available for radiation is higher than the power radiated it is given as follows:

$$\tilde{P}_{available} = \frac{E_{available}}{T_p} \quad (2.14)$$

Similarly the energy available is defined as:

$$E_{available} = \frac{1}{2\pi} \int_{-\infty}^{+\infty} E_s^{max}(\omega) d\omega \quad (2.15)$$

Material parameters and measurements mentioned in [20] and [21] were a reference to verify the results of Norton equivalent circuit implemented in the thesis work.

Table 2.1: Input and Output Parameters of the PCA Simulation Model.

Input Parameters	Output Parameters
N_x and N_y	$g(t)$
W_x , W_y and W_z	$i_g(t)$ and $I_g(\omega)$
Input laser details	R_g
Input laser average power	E_S
Semiconductor material properties	P_{rad} and $P_{available}$
V_{bias}	$\eta_m(\omega)$
Z_a	μ

2.2 Estimation of Detected Power - QO Channel Model

In the previous section, the Norton equivalent circuit model of a PCA implemented in the Matlab tool to quantify the power radiated by the PCA was described. Once the power radiated by the PCA and in turn, the power radiated by the transmitter is quantified, the next step in radar design is to estimate the power loss in the channel. For the emitted THz signals, such loss can be analyzed by resorting to the QO analysis for the propagation from the transmitter to the receiver. However, simulating the QO channel of the radar itself is not a great exercise as modeling the life sized QO components would be resource heavy and might not yield desirable results. Therefore, an alternate model is implemented in this thesis, the model has similar propagation mechanism to that of the desired radar scenario. Similar propagation mechanisms lead to a reasonable assumption that the involved efficiency terms calculated by the model will be similar to the ones observed in the real world scenario, which will give us an insight on the loss in the radar scenario. In this section, the QO model and the involved efficiency terms are explicitly discussed.

We use a commercial Menlo THz time-domain system, shown in Fig. 2.3, to study the QO channel. The Menlo system has an inbuilt laser power source and the laser pulse is aligned with the PCAs and the QO components in between. The schematic representation of the QO channel modelled after the Menlo THz time-domain system is shown in Fig. 2.4. The model implemented in the tool assumes a single PCA, coupled with a hemispherical lens, on the transmitter side and a horn antenna on the receiver side. We use two plano-convex Menlo lenses as the QO components in between the transmitter and the receiver.

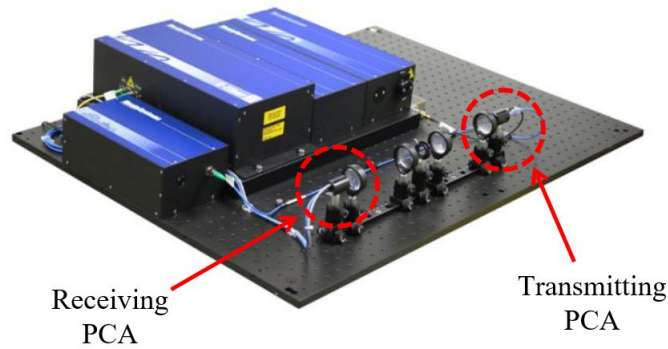


Figure 2.3: Menlo THz time-domain system. This device is commercially available with inbuilt laser power source.

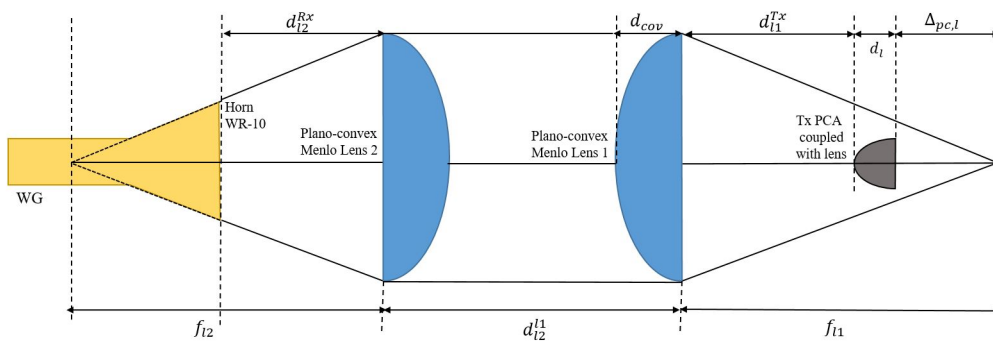


Figure 2.4: QO channel model implemented in the Matlab tool. The model consists of a PCA integrated with a hemispherical lens in Tx and two Menlo lenses to focus the transmitted power towards a horn antenna as a receiver.

The THz signal propagates from right to left in Fig. 2.4. On the rightmost side, a PCA radiates the THz signals into a hemispherical lens. The hemispherical lens focuses the THz signals on the plano-convex Menlo lens 1. The signal on reaching Menlo lens 2 from Menlo lens 1 is focused on the receiver horn antenna. The propagation path of the THz signal in the QO channel model can be better visualized from the ray tracing plot in the GRASP [22] simulation as presented in Fig. 2.5.

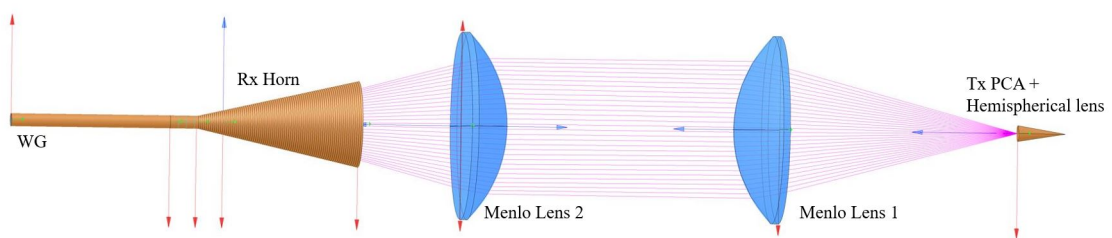


Figure 2.5: Ray tracing and QO channel model implemented in TICRA GRASP.

The primary objective of the QO channel model is to estimate all the QO efficiency terms in-

volved in the channel, and thus evaluating the detected power. The efficiency terms characterize the power loss at different QO components in the QO channel model. The power loss at these components is estimated by evaluating the input and output electric and magnetic fields at these components. Referring to Fig. 2.4, the QO components where the QO efficiency terms need to be estimated in order to estimate the detected power are: the PCA antenna, the hemispherical lens, Menlo lens 2, and receiver horn antenna.

Fig. 2.6 represents the process involved in the estimation of the QO channel efficiency through a block diagram. The PCA should be designed first in CST [23], where the electromagnetic (EM) fields radiated into the lens medium, referred to as the primary fields, can be obtained. Moreover, one can evaluate the front-to-back (f2b) efficiency of the PCA from the CST simulation. The primary fields are then radiated outside the hemispherical lens and propagated to the Menlo lens 1. These fields are referred to as the secondary fields and can be evaluated by using the physical-optics (PO) method. An in-house PO tool [18] is used to evaluate the secondary fields. The radiation efficiency of the lens can be obtained from the PO in Tx simulation performed on the lens. Finally, the secondary fields are focused by the Menlo lenses on the receiver horn antenna and this propagation path is simulated by the PO tool in TICRA GRASP [22]. This simulation returns the spillover efficiency of the QO system and also gives the electric and magnetic fields at the reception, by using which the detection efficiency can be calculated. These efficiencies together lead to the QO efficiency of the system which characterizes the QO channel loss and the power detected at the receiver.

It is worth mentioning that the PO approach is not applicable for frequencies below 100 GHz in our case. Therefore, we simulate the complete lens antenna in CST to obtain the secondary fields for frequencies below 100 GHz.

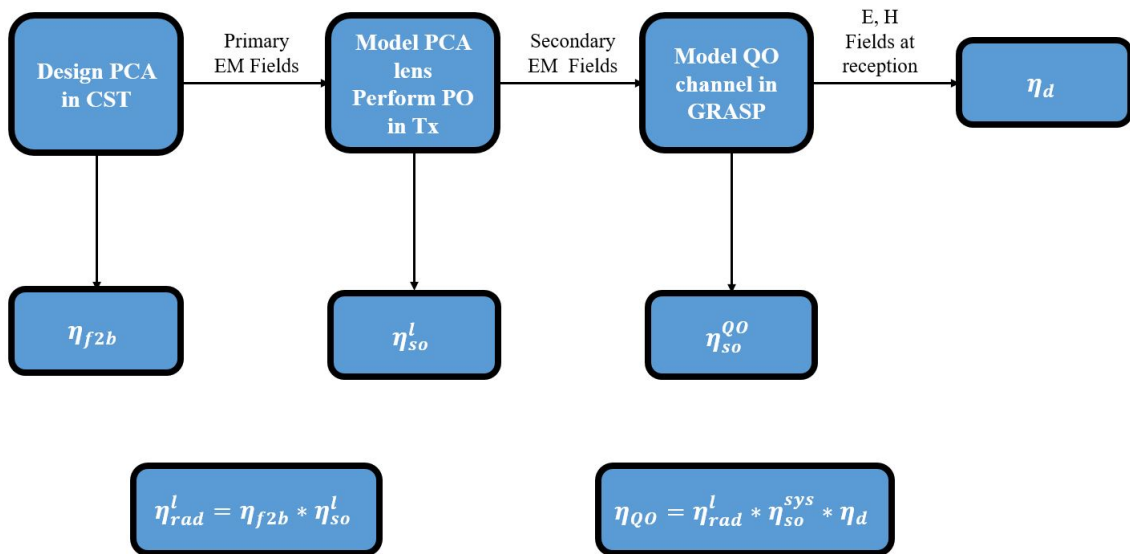


Figure 2.6: Block diagram that depicts the procedures to evaluate the efficiency terms in the QO model.

Until this point, the QO channel model and the process involved in the calculations of the power detected at the receiver and power lost in the channel were discussed. The efficiency terms involved in the QO channel analysis are discussed explicitly in the following sections. This analysis is divided into two parts: one is analysis of the hemispherical lens antenna and the other is the analysis of the QO path.

2.2.1 Analysis of the Lens Antenna

In our case, we consider a practical geometry that the PCA is integrated with a hemispherical lens, as shown in Fig. 2.7. In particular, the hemispherical lens used in this case is a hyperhemispherical lens [24] [25]. The extension, L , of the lens is given using:

$$L = \frac{R_{sph}}{\sqrt{\epsilon_r}} \quad (2.16)$$

where, R_{sph} is the radius of the spherical part of the lens, and ϵ_r is the permittivity of the lens dielectric. The PCA behaves as a feed of this lens and it is positioned at the focus, represented by \mathbf{O} in Fig. 2.7. The phase center (\mathbf{O}') of the lens lies outside of it, below the lens at a distance represented by Δ_{pc} , which is expressed as:

$$\Delta_{pc} = R_{sph}\sqrt{\epsilon_r} - L \quad (2.17)$$

where, L is the length of the extension given by, Eq. (2.16). In our case, the lens is designed in such a way that it's virtual focus aligns with the focus of the Menlo lens 1 in Fig. 2.4. A quarter-wavelength matching layer is employed to minimize the reflection at the lens-air boundary.

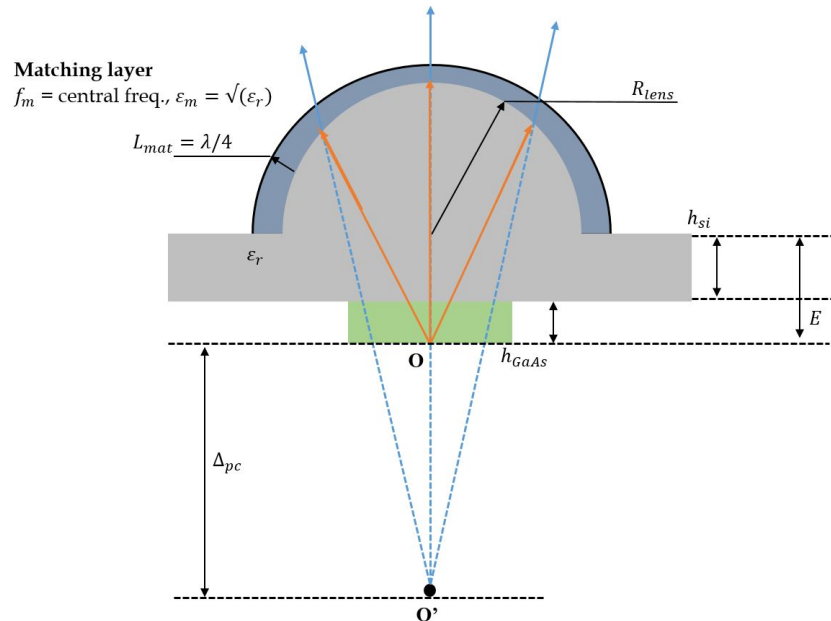


Figure 2.7: Hemispherical lens used in the QO Channel Model along with the ray tracing of EM fields radiated by the lens.

In Fig. 2.7, we can also see that the primary fields are represented by the orange rays. When these fields are transmitted outside the lens and radiated towards the Menlo lens 1, they are referred to as the secondary fields which are represented by the blue rays. It has to be noted that in the Fig. 2.7, the dimension are not in the real scale.

The power loss at the hemispherical lens is characterized by the radiation efficiency of the lens, which is defined as follows:

$$\eta_{rad}^l = \eta_{f2b} * \eta_{so}^{ant} * \eta_{ref}^l = \frac{P_{lens}}{P_{ant}} \quad (2.18)$$

where, P_{lens} is the power transmitted outside the lens which is calculated by integrating the EM fields on the lens surface as follows:

$$\vec{S}_{av}(\vec{r}) = \frac{1}{2} Re\{\vec{E}(\vec{r}) \times \vec{H}^*(\vec{r})\} \quad (2.19)$$

$$P_{lens} = \int \int \vec{S}_{av}(\vec{r}) \cdot \hat{n} dS = \int_0^{2\pi} \int_0^{\frac{\pi}{2}} \vec{S}_{av}(\theta, \phi) r^2 \sin(\theta) d\theta d\phi \quad (2.20)$$

where, r is the radial distance from the lens focus to the lens surface. P_{ant} is the total power radiated by the PCA in the whole sphere. Here it can also be seen that the radiation efficiency includes three terms. First is the front-to-back efficiency of the PCA which is defined as the ratio of the power radiated by the antenna in the upper hemisphere of the antenna to the total power radiated by the antenna in the whole sphere:

$$\eta_{f2b} = \frac{P_{ant}^u}{P_{ant}} \quad (2.21)$$

where, P_{ant}^u is the power radiated by the antenna in the upper hemisphere i.e. inside the lens, and P_{ant} is the total power radiated by the antenna in the whole sphere. It can be seen from the Eq. (2.21) that η_{f2b} quantifies how much power is radiated towards the lens surface. The second term in the radiation efficiency of the lens is the spillover of the PCA towards the lens surface, which can be calculated as follows:

$$\eta_{so}^{ant} = \frac{P_{ant}^{\theta_0}}{P_{ant}^u} \quad (2.22)$$

where, $P_{ant}^{\theta_0}$ is the part of the power radiated by the PCA inside the lens until the lens truncation angle. This term is a measures how much of the power radiated by the antenna is captured by the lens surface. And finally the reflection efficiency of the lens surface is evaluated. For a dielectric lens, we need to consider the reflection at the lens-air boundary, as well as the critical angle region where total reflection occurs. The reflection of the EM fields at the lens-air boundary takes place according to the Snell's law and Fresnel law. To improve the reflection

efficiency, as mentioned before, we can use a quarter wavelength matching layer at the lens surface to minimize the reflection at the lens-air boundary. The reflection efficiency, η_{ref}^l is then expressed as:

$$\eta_{ref}^l = \frac{P_{lens}}{P_{ant}^{\theta_0}} \quad (2.23)$$

where, P_{lens} is the power radiated outside the lens surface.

To make the analysis clearer, here we can combine the antenna spillover efficiency and the reflection efficiency and define it as the spillover efficiency of the lens:

$$\eta_{so}^l = \eta_{so}^{ant} * \eta_{ref}^l = \frac{P_{lens}}{P_{ant}^u} \quad (2.24)$$

Then, the radiation efficiency of the lens becomes:

$$\eta_{rad}^l = \eta_{f2b} * \eta_{so}^l \quad (2.25)$$

2.2.2 Analysis of the QO Path

In the previous part of the chapter, the hemispherical lens was analyzed and the lens radiation efficiency characterizing the power loss at the hemispherical lens was explained. In this part, the rest of the QO path is discussed and the power detected at the receiver and the power loss in the channel is characterized.

In Fig. 2.5, it can be seen that the hemispherical lens focuses the THz signal towards the Menlo lenses. It is explained previously that the virtual focus hemispherical lens is aligned with the focus of the Menlo lens 1. As a result, Menlo plano-convex lens 1 can then produce nearly collimated rays and Menlo lens 2 can focus well those rays on the horn.

To characterize the power detected at the horn, we simulated the whole QO path in TICRA GRASP, with the lens secondary fields as the tabulated source. The simulation yields the EM fields detected at the receiver along with the spillover efficiency of the dual Menlo lens system which characterizes the power reaching the receiver. The power detected is estimated from the EM fields evaluated at the receiver. The detection efficiency characterizes the detected power. Finally, QO efficiency of the complete channel, which characterizes the power loss in the complete channel, is estimated. Subsequent sections describe these efficiencies in detail.

2.2.2.1 Spillover efficiency of the QO system

In Fig. 2.5, the propagation of the THz signal from the PCA lens antenna to the Menlo lens 2 introduces the spillover efficiency of the QO system, which quantifies how much power is captured by the second Menlo lens for the specific QO path:

$$\eta_{so}^{sys} = \frac{P_{M2}}{P_{lens}} \quad (2.26)$$

where, P_{lens} is the power radiated by the hemispherical lens and P_{M2} is the power captured by the second Menlo lens. P_{M2} is estimated using the PO tool in GRASP. The Matlab tool can therefore directly read η_{so}^{sys} from the simulation and process it.

2.2.2.2 Detection efficiency of the horn

Detection efficiency of the receiver horn quantifies the power received by the horn in Rx and it is evaluated using the equation given below:

$$\eta_d = \frac{P_d}{P_{M2}} \quad (2.27)$$

where, P_d is the power detected by the receiver horn. This power is calculated by integrating the Poynting vector inside the waveguide (WG) of the horn in GRASP. Fig. 2.8 shows the circular grids inside the waveguide where the Poynting vector along with the received electric and magnetic fields are estimated in the GRASP simulation. It has to be noted that in GRASP only a body of revolution can be modelled, therefore, we have a circular waveguide in the simulation. The power detected is then expressed as:

$$P_d = \int_0^{\rho_0} \int_0^{2\pi} \vec{S}_{x,y,z} \cdot \hat{z} \rho d\rho d\phi \quad (2.28)$$

where, $\vec{S}_{x,y,z}$ is the Poynting vector on the circular grid inside the WG in the GRASP simulation.

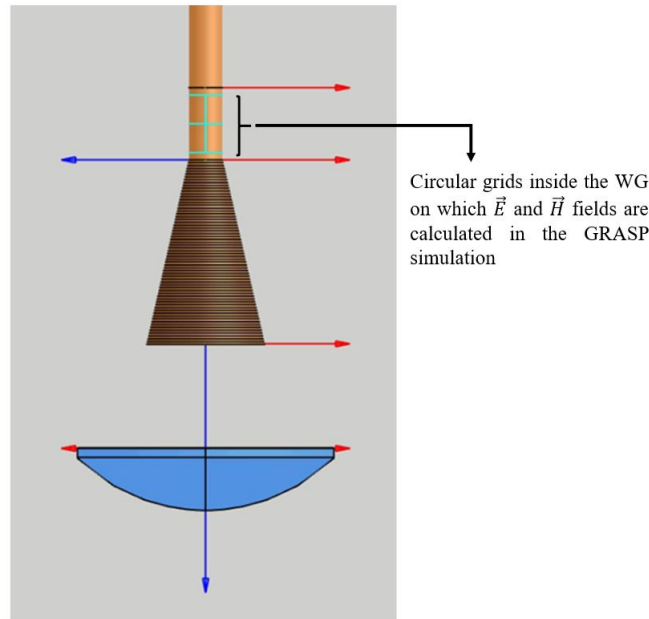


Figure 2.8: Detector of the QO channel model simulation in GRASP. \vec{E} and \vec{H} fields are calculated on the circular grid (represented by horizontal green markings in the figure) inside the waveguide.

2.2.2.3 QO efficiency of the complete system

The QO efficiency of the complete channel characterizes the power loss in the complete channel and it is expressed as:

$$\eta_{QO} = \eta_{rad}^l * \eta_{so}^{sys} * \eta_d \quad (2.29)$$

As mentioned previously, the QO efficiency estimated in the QO channel model can give us an idea of the power loss when the radar scenario is considered. If the QO efficiency of the channel is known and the power transmitted is known as well, the energy received at the receiver can be given as below:

$$E_d = \eta_{QO}(\omega) * E_s^{Tx} \quad (2.30)$$

where, E_s^{Tx} is the energy spectrum of the transmitted THz signal. The power detected at the receiver can be obtained from the energy received by the receiver.

Chapter 3

The Matlab GUI Tool

In the previous chapter, we discussed the circuit model of the PCA and the QO channel model along with their theoretical background. In this chapter, the designed Matlab tool is discussed in detail. As mentioned before the Matlab tool is divided into three parts. The first part of the tool is referred to as the "Transmitter interface" which models the Norton equivalent circuit of the PCAs and estimates the power radiated by the PCA along with other important parameters such as the conductance of or the current across the semiconductor gap of the PCA. Moreover, a connected array of PCAs, similar to the one in [16], can also be analyzed in the transmitter interface. The second part of the Matlab tool is the "QO Channel Analyzer interface", this interface simulates the QO channel model in Fig. 2.4 to estimate the QO channel efficiency that characterizes the power detected at the receiver and the power loss in the channel. Finally the third part of the tool is referred to as the "Main interface" of the tool which deals with the detection and imaging related parameter estimation on a system level when the Tx and QO channel parameters are obtained from the first two interfaces. The first two interfaces can be accessed from the main interface of the tool and the radiated power calculated in the transmitter interface can be exported to the main interface to obtain estimation of detection and imaging related parameter with a greater accuracy. Similarly, QO channel analyzer interface can assist in estimation of the radar parameters in the main interface as well.

The subsequent sections of this chapter describe the different parts of the Matlab tool. To explain the utility of the Matlab tool a Bow-tie antenna in [21] is used as a PCA.

3.1 Transmitter Interface

In Fig. 3.1 the "Transmitter Interface" of the Matlab tool is shown. The inputs are outputs are separated with the dashed boxes in the figure. As stated earlier, this interface can be accessed from the main interface of the tool. The Norton circuit of the PCAs is implemented in this interface and with the given inputs this interface can estimate the power radiated by the

PCAs along with other important quantities such as the conductance and current across the PCA semiconductor gap. In this section we discuss the transmitter interface in detail by following the dashed boxes in Fig. 3.1 one by one.

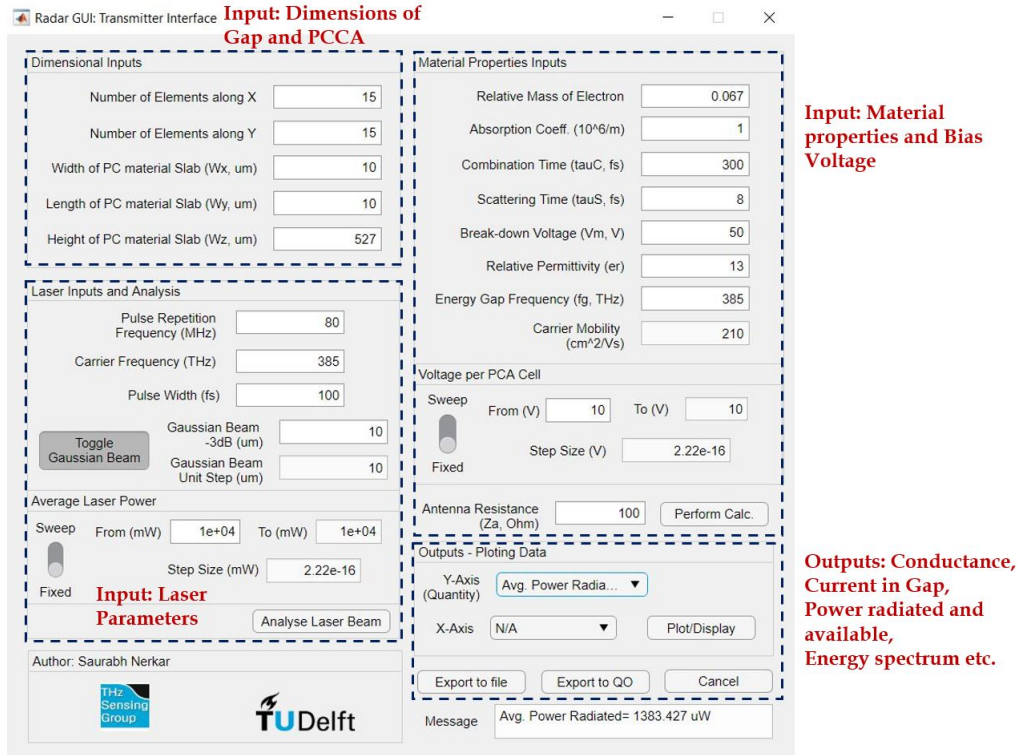


Figure 3.1: The "Transmitter interface" of the Matlab tool.

The utility of the interface is explained using a Bow-tie antenna in [21] as the PCA. The schematic of the Bow-tie antenna is shown in Fig. 3.2. The semiconductor gap of the Bow-tie antenna is made up of Gallium Arsenide (GaAs) which has a relative permittivity of 12.4 and the antenna radiates into the silicon hemispherical lens which has a relative permittivity of 11.9. The frequency of operation of the antenna is 20 GHz to 1900 GHz.

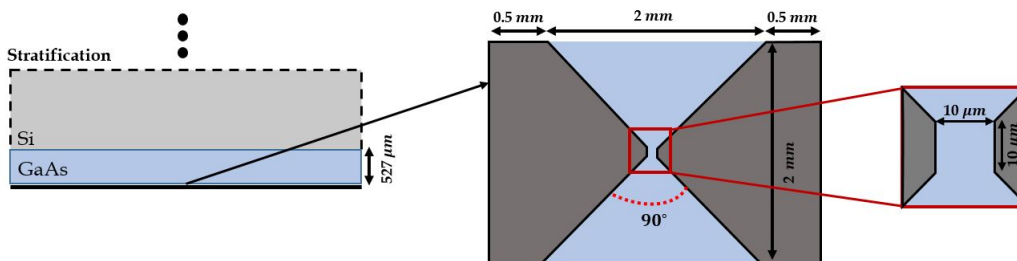
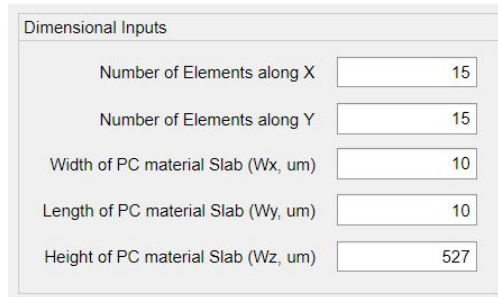


Figure 3.2: Stratification, top view and the semiconductor gap of the Bow-tie antenna used as a PCA to explain the utility of the Matlab tool.

3.1.1 Input: Dimensions of the Gap and the connected array of PCAs

Fig. 3.3 shows a section of the transmitter interface which takes the dimensional inputs for a single PCA gap or if the number of PCAs is larger, it takes the dimensions of a single PCA in $N_x \times N_y$ connected array of the PCAs.



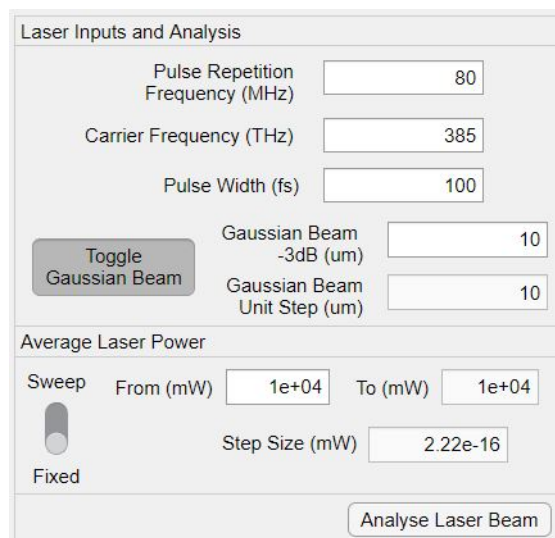
Dimensional Inputs	
Number of Elements along X	15
Number of Elements along Y	15
Width of PC material Slab (Wx, um)	10
Length of PC material Slab (Wy, um)	10
Height of PC material Slab (Wz, um)	527

Figure 3.3: Tx interface input: Dimensions of the semiconductor gap and the connected array of the PCAs

The section of the transmitter interface shown in Fig. 3.3 expects the width, W_x , length, W_y and height/thickness, W_z of the single PCA semiconductor gap along with the number of elements, $N_x \times N_y$ in x and y direction in the connected array of the PCAs if there are more than one PCA. The dimensions of PCA semiconductor gap and the dimensions of the PCA connected array play an important role in determining the power transmitted by a PCA in Tx. Fig. 3.3 showcases a 15×15 array of Bow-tie antennas described earlier. For the Bow-tie PCA the semiconductor gap has dimensions $10\mu\text{m} \times 10\mu\text{m} \times 527\mu\text{m}$. The power radiated by this setup is discussed in the output section described later in the chapter.

3.1.2 Input: Laser Details

Fig. 3.4 shows the section of the Tx interface where the values of different parameters of the laser impinging on the PCA can be given.



Laser Inputs and Analysis	
Pulse Repetition Frequency (MHz)	80
Carrier Frequency (THz)	385
Pulse Width (fs)	100
<input type="checkbox"/> Toggle Gaussian Beam	
Gaussian Beam -3dB (um)	10
Gaussian Beam Unit Step (um)	10
Average Laser Power	
Sweep	<input type="checkbox"/>
From (mW)	1e+04
To (mW)	1e+04
Step Size (mW)	2.22e-16
Fixed	<input type="checkbox"/>
<input type="button" value="Analyse Laser Beam"/>	

Figure 3.4: Tx interface input: Laser details.

The laser impinging on the PCA is an important part of the THz power generation using the PCA as it is one of the factors that determine the THz power radiated by the PCA. The laser parameters expected by the Tx interface are: pulse repetition frequency (PRF), f_p , carrier frequency, τ_c , pulse width, τ_p , and the average laser power, P_{laser} . The expected units of these parameters can be seen in the Fig. 3.4. Apart from these, the interface also expects the beam power distribution of the laser. The radius of the beam can be specified directly if the beam power distribution is uniform or -3 dB radius can be specified if the beam power distribution is Gaussian.

Notably, "Laser Analysis interface" can analyze the given laser signal to understand its power spectral density and the spatial distribution of its electric field. This interface can be accessed using the "Analyze Laser Beam" button on the Tx interface which can be seen in Fig. 3.4. The details of this interface are given in Appendix A.

One of the limitations of the Matlab tool can be seen here. The limitation is that the laser power taken as input is assumed to be distributed equally amongst the elements of the connected array of the PCAs. In an ideal scenario, a micro-lens array will be utilized to work out the distribution of power amongst the PCA connected array elements.

The input values of the laser parameters shown in 3.4 are utilized with the Bow-tie PCA connected array setup. The results from this setup are discussed later in the chapter.

3.1.3 Input: Material Properties and Bias voltage

Apart from the laser impinging on the semiconductor gap, the semiconductor gap material itself is very important for determining the power radiated by the PCA. Fig. 3.5 shows a section of the transmitter interface where the values of the different PCA semiconductor gap material properties, bias voltage, V_{bias} , applied to a single PCA cell to excite the carriers in the semiconductor gap after the laser impinges on it, and the resistance of the antenna, Z_a , should be provided.

The PCA semiconductor gap material properties that can be provided as inputs in this section of the Tx interface are:

- the relative mass of the electron in the semiconductor material, m_e
- the absorption coefficient of the material, α , which is a measure of the material's ability to absorb the EM radiation
- combination time, τ_c which is the average value of lifetimes of all different kind of recombination phenomena in a semiconductor material [20]
- scattering time, τ_s which is the time taken by a carrier in a semiconductor, where the carrier is in motion due to external electric field, before it collides with something else and changes its motion

- breakdown voltage, V_m , is the limit of the bias voltage that can applied to the semiconductor material above which the thermal breakdown of the material takes place
- relative permittivity, ϵ_r
- energy gap frequency, f_g , which gives the the energy, $E = hf_g$, required to move the charge carrier from valance band to conduction band in a semiconductor where, h is the Plank's constant.

Figure 3.5: Tx interface input: PCA semiconductor gap material properties and bias voltage applied to the PCA unit cell in the PCA array.

The units of the required quantities are mentioned explicitly in the interface and can be seen in Fig. 3.5. The values in the figure belong to the semiconductor material, LT-GaAs, of the Bow-tie antenna that is used as PCA as mentioned before in the chapter. Table 3.1 summarizes the material properties of the semiconductor gap material for the Bow-tie antenna.

Table 3.1: Summary of the semiconductor gap material details for the Bow-tie antenna.

Parameter	Value
Relative mass of electron	0.067
Absorption coefficient	$1 \times 10^6 m^{-1}$
Combination time	300 fs
Scattering time	8 fs
Relative permittivity	13
Energy gap frequency	385 THz
Antenna resistance	100 Ω

3.1.4 Outputs

As discussed earlier, the purpose of the transmitter interface of the Matlab tool is to implement the Norton equivalent circuit of the PCAs and quantify the power radiated by the (connected array of) PCAs in the given conditions. The average power radiated by the PCA and estimated in the transmitter interface can be exported to the Matlab tool's main interface or if the user desires the entire work-space can be exported to a Matlab data file as well.

The mathematical analysis behind various outputs of the transmitter interface i.e. multiple parameters related to the Norton circuit of the PCA is discussed in section 2.1. Fig. 3.6 represents the section of the Tx interface that can be used to access the output parameters of the analysis of the Norton circuit of the PCA performed with given input parameters.

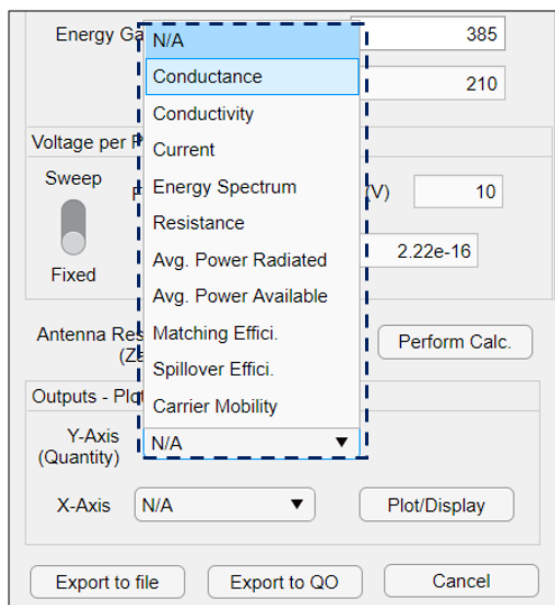


Figure 3.6: Tx interface output: the section of the Tx interface that provides access to the outputs obtained.

The output parameters of the analysis of the Norton equivalent circuit performed using the transmitter interface are:

- behaviour of the conductance, g , across the semiconductor gap with respect to time and frequency
- behaviour of the current, i , across the the semiconductor gap with respect to time and frequency
- behaviour of the conductivity, σ , across the semiconductor gap with respect to time and frequency
- energy spectrum, E_s , of the energy radiated by a single PCA
- gap resistance, R_g , of the semiconductor gap calculated as a function of the input laser power or input bias voltage

- average power available, P_{avail} , for the radiation at the given PCA
- average power radiated, P_{rad} , by the (connected array of) the PCAs
- matching efficiency, η_m , of the PCA
- spillover efficiency of the laser beam, η_{so}^{laser} , which is the measure of the laser power loss when the area of the laser beam is larger than the area of the PCA semiconductor gap, details of this parameter are discussed in Appendix A.

Let's analyze the results obtained from the transmitter interface for a single Bow-tie antenna and different input parameters. The constant parameters of the Bow-tie antenna in the analysis can be summarized in Table 3.2.

Table 3.2: Summary of the constant parameters of the Bow-tie antenna analyzed using the transmitter interface.

Parameter	Value
Gap dimensions	$10\mu m \times 10\mu m \times 527\mu m$
Laser PRF	80 MHz
Laser carrier frequency	385 THz
Laser pulse width	100 fs
Laser beam -3 dB radius	$10\mu m$
Relative mass of electron	0.067
Absorption coefficient	$1 \times 10^6 m^{-1}$
Combination time	300 fs
Scattering time	8 fs
Relative permittivity	13
Energy gap frequency	385 THz
Antenna resistance	100 Ω

In Fig. 3.7, we can see the power radiated by the PCA as a function of the input laser power. It can be seen in the figure that the power radiated by the PCA increases with the increase in the input laser power and saturates after a point. This is because the gap semiconductor material properties, e.g. absorption coefficient, responsible for the generation of the THz signals from the impinging laser are finite. In the case of the Bow-tie antenna, the increment in the power radiated with respect to the increase in laser power slows down after 100 mW of input laser power and saturates at around 700 mW of input laser power. Similarly, Fig. 3.8 shows the power radiated by the PCA as a function of the bias voltage applied to the PCA. The power radiated by the PCA increases with the increase in the bias voltage and saturates after a point, however, because the bias voltage has to be lower than the breakdown voltage of the semiconductor material, saturation might not occur as the bias voltage will never cross a specific value.

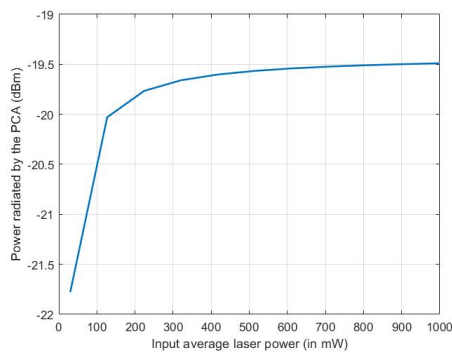


Figure 3.7: Power radiated by the PCA as a function of the input average laser power.

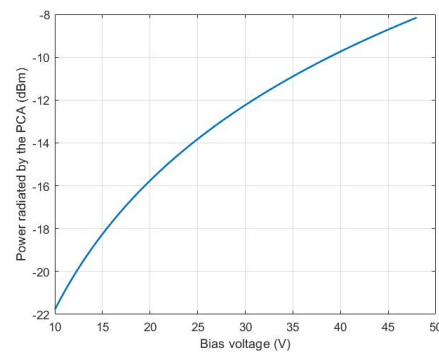


Figure 3.8: Power radiated by the PCA as a function of the bias voltage applied to the PCA.

Fig. 3.9 and Fig. 3.10 represent the energy spectrum of the radiated THz signal for different values of the input laser power and different values of the bias voltage respectively. Similar to the power radiated results described in the previous paragraphs, the energy radiated is higher for the higher values of the input power and bias voltage.

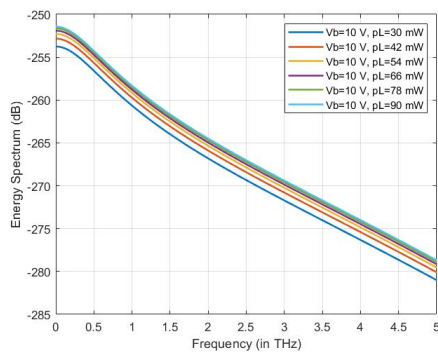


Figure 3.9: Energy spectrum of the radiated THz signal for different values of input laser power.

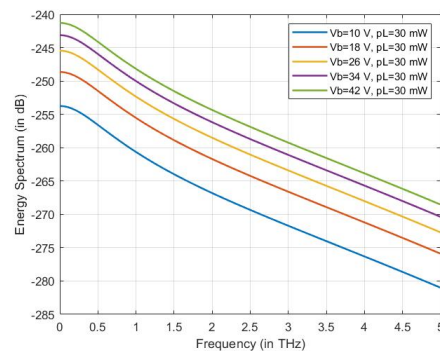


Figure 3.10: Energy spectrum of the radiated THz signal for different values of the bias voltage applied to the PCA.

Fig. 3.11 and Fig. 3.12 represent the semiconductor gap resistance as a function of the input laser power and the voltage respectively. From Eq. (2.8) we know that the gap resistance is inversely proportional to the input laser power and it is independent of the bias voltage. This can be seen in the respective figures. As the matching efficiency is a function of the gap resistance, it shows a similar behaviour as that of the gap resistance.

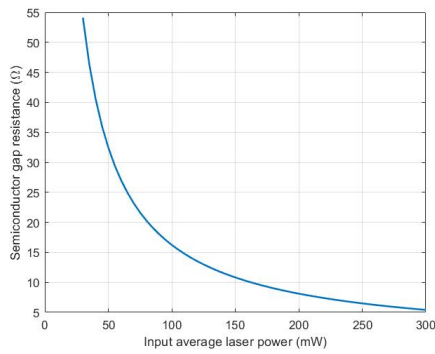


Figure 3.11: Semiconductor gap resistance of the PCA as a function of the input laser power.

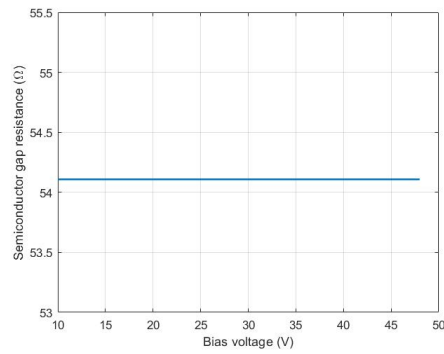


Figure 3.12: Semiconductor gap resistance of the PCA as a function of the bias voltage.

Now, let's look at the current induced across the semiconductor gap. Fig. 3.13 and Fig. 3.14 show the current induced across the semiconductor gap w.r.t. time for different values of the input laser power and bias voltage respectively. It can be seen in the figures that, the increasing the value of the laser power or the voltage increases the current induced. The current is induced only for a short duration because of the specific value of the combination time and scattering time of the material which leads to a specific charge carrier mobility.

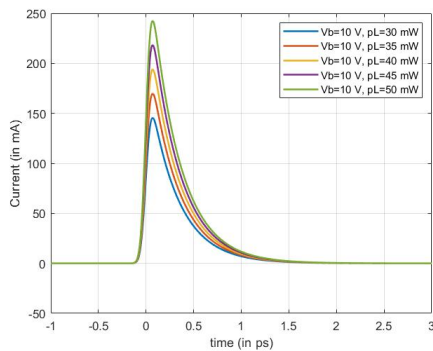


Figure 3.13: Current induced across the semiconductor gap w.r.t. time for different values of the input laser power.

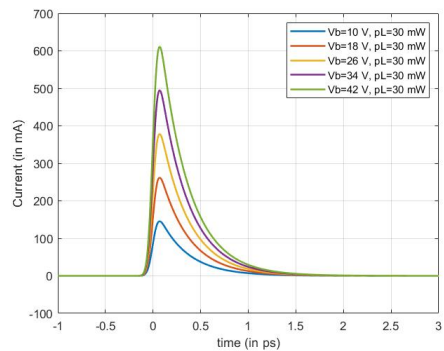


Figure 3.14: Current induced across the semiconductor gap w.r.t. time for different values of the bias voltage.

Fig. 3.15 represents the spectrum of the current induced across the semiconductor gap of the PCA. Fig. 3.16 shows the conductance across the semiconductor gap w.r.t. time for different values of the input laser power. The conductance behaves similar to the current in Fig. 3.13. The spectrum of the current and the conductance are useful in the estimation of the power radiated by the PCA in frequency domain. The conductance is unaffected by the change in the bias voltage similar to the gap resistance.

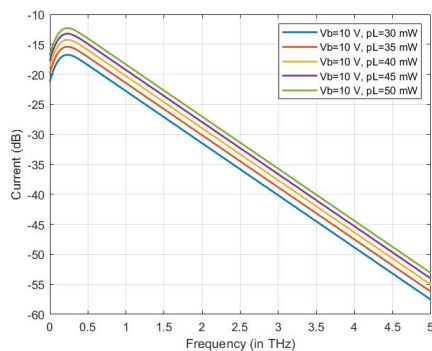


Figure 3.15: Current induced across the semiconductor gap w.r.t. frequency for different values of the input laser power.

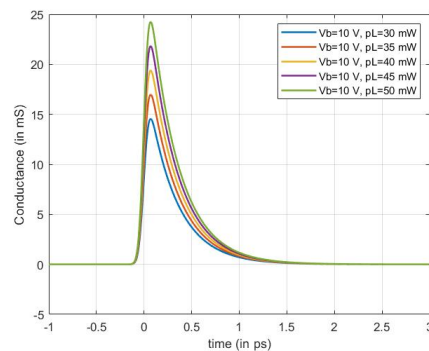


Figure 3.16: Conductance across the semiconductor gap w.r.t. time for different values of the input laser power.

Until this point, we analyzed a single Bow-tie PCA. We understood the effect of various material parameters and the input laser power along with the effect of the bias voltage applied to the PCA on the output parameters such as the power radiated, energy spectrum, current and conductance across the gap. Moving forward, let's note that the power radiated by a Bow-tie array with 15×15 antenna elements, the material properties and dimensional inputs as specified above lead to $1.38mW$ of radiated THz power, provided the bias voltage of the PCA cell is 10 V and laser power impinging on each of the PCA in the array is around 44 mW. This power will be used as the transmitted THz power in the main interface for estimating the detection and imaging parameters. Another important point to be noted is that the results obtained from the transmitter interface are similar to the results in the study [20] for similar input parameters validating the Norton circuit model implemented in the transmitter interface. However, the methods to evaluate some of the parameters is different in the thesis from the study in [20].

3.2 QO Channel Analyzer Interface

Fig. 3.17 shows the "QO Channel Analyzer" interface of the Matlab tool also referred to as the QO channel interface in the thesis. We can see that the interface is user-friendly and the inputs and outputs are separated with the dashed boxes in the figure similar to the previous sections. This interface is accessible to the user through the main interface of the tool. The user can access this interface by pressing the "QO Channel Analyzer" button on the main interface of the tool. This interface implements the QO channel model described in section 2.2 and estimates different efficiencies related to different QO components in the channel model. These efficiencies together characterize the detected power at the receiver and the power loss in the QO channel. In this section, we discuss the QO channel analyzer interface in detail following the dashed boxes one by one. As mentioned in the previous section, the utility of the tool is explained by using the Bow-tie antenna depicted in Fig. 3.2 as the PCA.

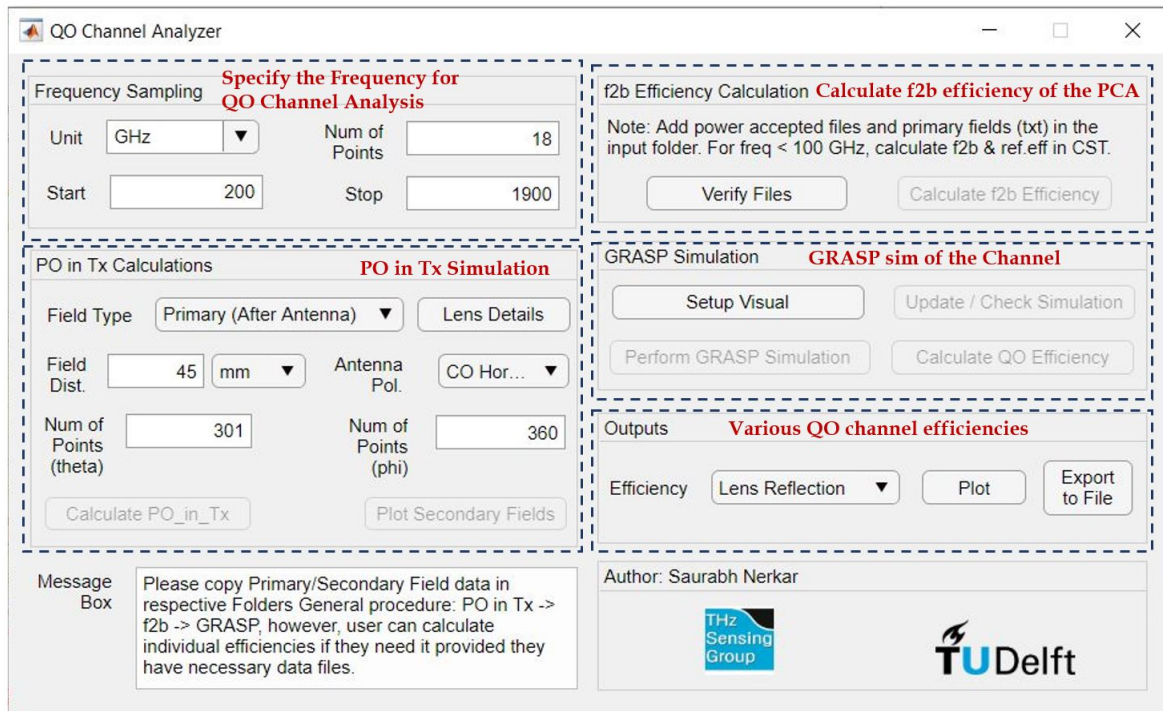


Figure 3.17: QO Channel Analyzer interface of the Matlab tool: the inputs and outputs are separated by the dashed boxes, this interface estimates the QO efficiency of the complete channel.

We have seen the process of estimation of the QO channel efficiency in section 2.2. Multiple different simulations viz., the CST, PO in Tx, and GRASP, are needed to estimate the EM fields at different QO components in the QO channel model. The QO channel interface automates these simulations and makes the QO efficiency estimation easy and user-friendly. Different sections of the QO channel interface belong to different simulations involved. Therefore, each section of this interface has a set of inputs and a set of outputs. Let's follow the dashed boxes and understand the utility of the interface in detail.

3.2.1 Frequency Sampling

Fig. 3.18 shows the section of the QO channel interface that takes the frequencies where the QO channel model needs to be simulated as the inputs. The "start" frequency, the "stop" frequency and "number of points" can be specified. The unit of the frequency specified can be chosen by the user.



Figure 3.18: Frequency sampling section of the QO channel interface where the frequencies for which the QO channel model need to be simulated are specified.

3.2.2 PO Simulation

As seen in the section 2.2, the first step in the analysis of the QO channel model is to estimate the power loss at the hemispherical lens. The PO simulation is performed on the primary fields to estimate the spillover efficiency of the hemispherical lens. The spillover efficiency of the hemispherical lens along with the f2b efficiency of the antenna characterizes the THz power loss at the hemispherical lens.

Fig. 3.19 represents the section of the QO channel interface that deals with the PO simulation of the hemispherical lens. This section performs two tasks:

1. Take inputs of the primary fields and perform PO in Tx simulation on the hemispherical lens.
2. If the PO simulation has been already performed verify the secondary fields according to the given inputs.

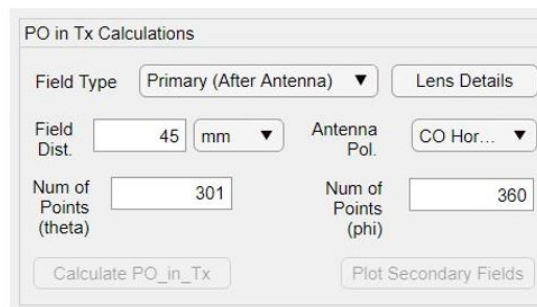


Figure 3.19: PO simulation section of the QO channel interface of the Matlab tool.

From Fig. 3.19 it can be seen that the interface of the PO simulation is simple. Once the necessary field files are made available in the specific directories the users have to provide the following inputs to perform the simulation:

- **Field Type:** The users can chose the type of field they are providing in the folders i.e. primary fields or secondary fields. In case the primary fields are provided, the interface runs the PO simulation and estimates the spillover efficiency of the lens along with the secondary fields. In case the secondary fields are provided, the interface does not run the PO simulation, instead only verifies whether the necessary secondary field files exists for GRASP simulation.
- **Lens Details:** The users have to provide the hemispherical lens details, for example, the rim angle, permittivity of the lens material etc. The lens details of the hyperhemispherical lens used with the Bow-tie PCA is shown in Fig. 3.20.
- **Field Dist.:** This is the distance from the lens surface where the users want to estimate the secondary fields. Sometimes the distance between the Menlo lens and the PCA is too short, in the near field region.

- **Antenna Polarization:** The users must provide the antenna polarization. It can be known from the CST simulation of the PCA. The Ludwig definitions [26] of the polarization are utilized for the calculations.
- **Resolution of the simulation:** Number of points in θ and ϕ provided by the user are used to estimate the secondary fields in the PO simulation. The simulation might not give appropriate results if these points are less. The default values given in the interface are ideal.

The PO simulation outputs the spillover efficiency, η_{so}^l , of the lens which can be accessed using the output section of the QO channel interface.

In this interface, we provided the primary fields of the mentioned Bow-tie antenna and estimated the secondary fields at 45 mm distance from the lens. The hemispherical lens used in the QO channel model is shown in Fig. 3.20. For this example, the radius of the lens is 5 mm, the rim angle is 73.83° , the extension is 1.45 mm, Silicon is taken as the lens dielectric ($\epsilon = 11.9$) and a matching layer with 400 GHz as the central frequency is employed. The matching layer is not shown in the figure.

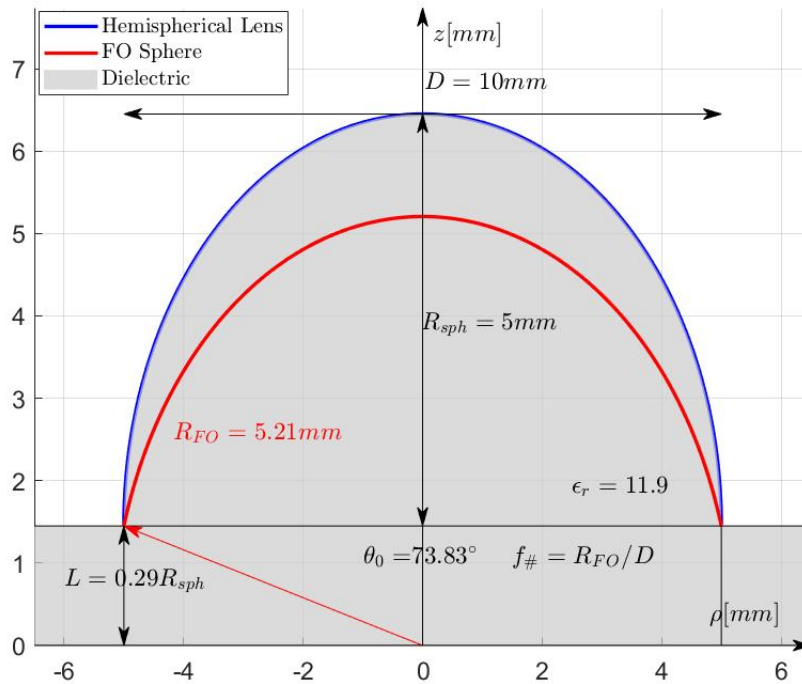


Figure 3.20: The hyperhemispherical lens geometry used with Bow-tie antenna PCA and plotted using the Lens Details interface of the Matlab tool. This geometry does not show the matching layer.

The antenna polarization was CO-Horizontal and the simulation was performed over a frequency range of 200 GHz to 1900 GHz. Fig. 3.21 shows the spillover efficiency of the hemispherical lens, η_{so}^l . Fig. 3.22 and Fig. 3.23 presents the secondary fields radiated by the lens

at 500 GHz and 1000 GHz respectively. It can be seen from Fig. 3.21 that the Bow-tie antenna coupled with this hemispherical lens has an average spillover efficiency of 0.6, which is not ideal for many applications and most of the power loss in the channel might be happening at the hemispherical lens itself. Fig. 3.22 and Fig. 3.23 give an insight that at higher frequencies the Bow-tie antenna does not have a good broadside radiation. Leaky wave antenna can be investigated in future as it can be a good replacement of the Bow-tie in the QO channel model.

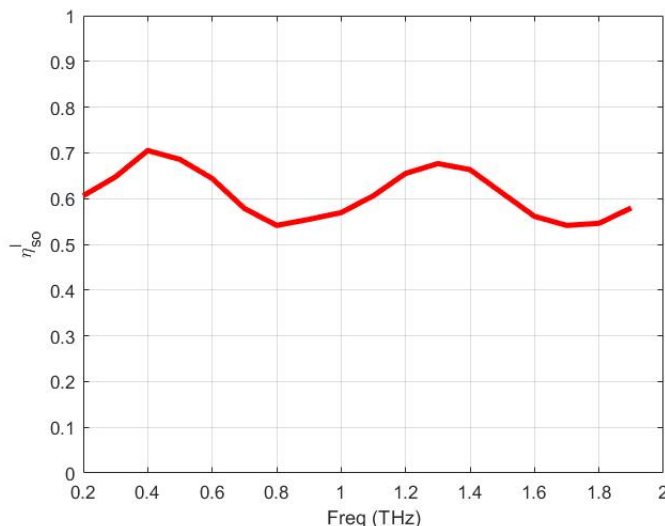


Figure 3.21: Spillover efficiency of the hemispherical lens estimated by the PO in Tx simulation.

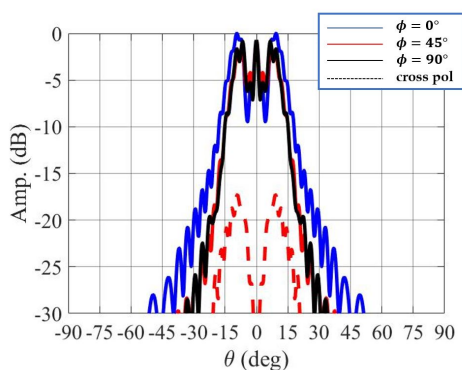


Figure 3.22: Secondary electric field radiated at 500 GHz by the hemispherical lens estimated by the PO in Tx simulation.

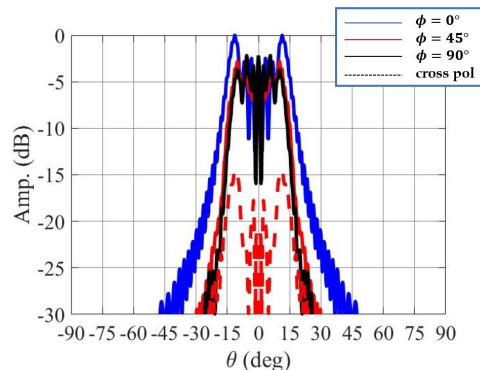


Figure 3.23: Secondary electric field radiated at 1000 GHz by the hemispherical lens estimated by the PO in Tx simulation.

In Eq. (2.25), we saw that the radiation efficiency of the lens has two terms: one the spillover efficiency of the lens, η_{so}^l and the f2b efficiency of the antenna, η_{f2b} . The section of the QO channel interface shown in Fig. 3.19 estimated the spillover efficiency of the lens. The f2b efficiency of the antenna is estimated in the section of the QO channel interface shown in Fig. 3.24.

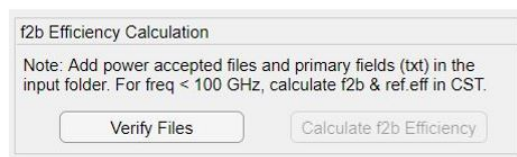


Figure 3.24: f2b efficiency calculation section of the QO channel interface.

The f2b efficiency evaluated for the Bow-tie PCA is presented in Fig. 3.25. It can be noted from the graph that the Bow-tie antenna has an excellent f2b efficiency i.e. most of the power, out of the total power radiated by the antenna, is radiated inside the lens.

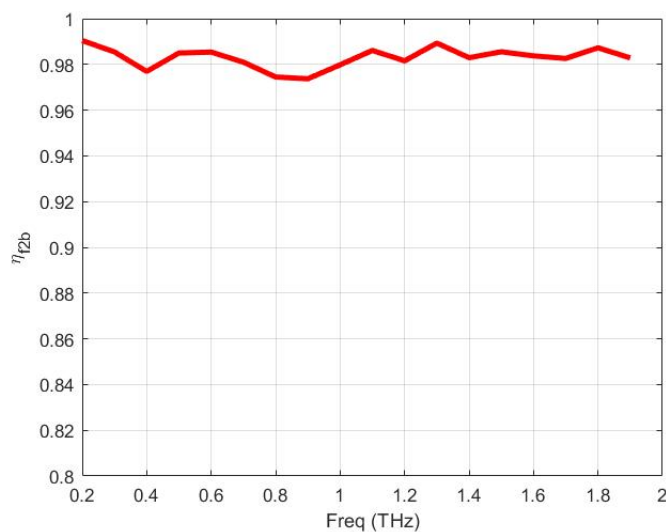


Figure 3.25: f2b efficiency of the Bow-tie PCA.

The radiation efficiency of the lens, η_{rad}^l is shown in Fig. 3.26. As the Bow-tie has excellent f2b efficiency, the radiation efficiency is almost identical to the spillover efficiency of the lens. Therefore, it can be said that, for Bow-tie hemispherical lens system, the radiation efficiency is not ideal and most of the power loss might be happening at the hemispherical lens itself.

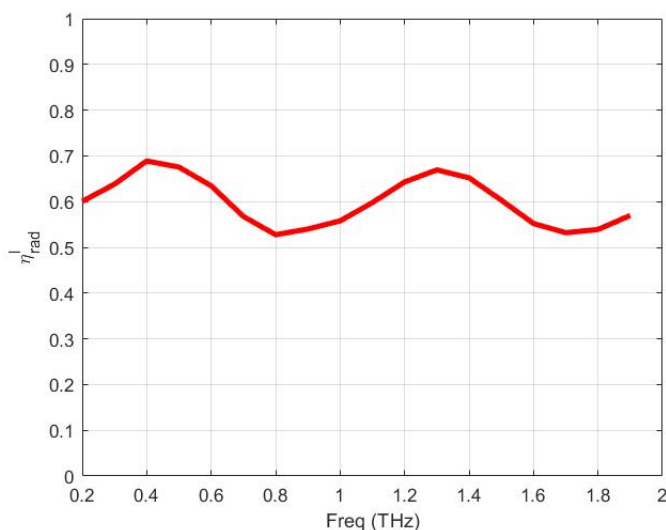


Figure 3.26: Reflection efficiency, η_{rad}^l of the hemispherical lens.

It has to be noted that the radiation efficiency of the PCA is very important when quantifying the loss in a radar scenario, which will be discussed in the next section.

The hemispherical lens used in the example is shown in Fig. 2.7. The lens details were input using the "Lens Details" interface, this interface can be accessed using the "Lens Details" button on the QO channel interface, PO in Tx section, in Fig. 3.19. Fig. 3.27 shows the Lens Details interface. The interface is simple and user-friendly.

The screenshot shows a window titled "Lens Details" with a standard Windows-style title bar (minimize, maximize, close buttons). The window contains two main sections: "Lens Details" and "Matching Layer Details".

Lens Details Section:

- Lens Type:** A dropdown menu set to "Hemispherical Lens".
- Diameter:** A text input field containing "10" and a unit dropdown set to "mm".
- Rim Angle (deg):** A text input field containing "73.83".
- Extension (R_sph):** A text input field containing "0.29".
- F number:** A text input field containing "0.521".
- Permittivity:** A text input field containing "11.9".
- Phase Center:** A text input field containing "15.8" and a unit dropdown set to "mm".
- Plot Surface:** A button located below the input fields.

Matching Layer Details Section:

- Enable:** A checked checkbox.
- Material:** A text input field containing "2.72".
- Frequency:** A text input field containing "400" and a unit dropdown set to "GHz".
- Load Lens Details:** A button located at the bottom of the section.

Figure 3.27: Lens details interface which takes the lens details as inputs from the user. It can be accessed from the QO channel interface.

It has to be noted that the PO in Tx simulation does not give accurate results for frequencies less than 100 GHz. Therefore, for frequencies less than 100 GHz, we simulate the hemispherical lens in CST itself along side the Bow-tie PCA and evaluate the secondary fields directly, the radiation efficiency of the lens can also be estimated in CST in such a scenario. The evaluated secondary fields are then utilized in GRASP simulation to estimate the detection efficiency and the spillover efficiency of the dual Menlo lens system in the QO channel model.

3.2.3 GRASP Simulation

We have seen in the previous chapter that once the hemispherical lens is analyzed using the PO simulation and the rest of the QO path is simulated in GRASP. The QO channel model that is simulated in GRASP is shown in Fig. 2.4. The GRASP simulation takes the secondary fields as tabulated source and estimates the spillover efficiency of the dual menlo lens system and the detection efficiency. After estimating the radiation efficiency of the hemispherical lens, the

spillover efficiency of the dual menlo lens system and the detection efficiency of the receiver horn, the QO channel efficiency is evaluated using Eq. (2.29). Using the QO efficiency the power loss in the channel and the power detected at the receiver can be characterized. The user can utilize these efficiencies in the Main interface of the Matlab tool to estimate the power loss in the channel. However, it has to be noted that the QO channel model implemented in the QO channel interface does not account for the power loss from the reflection of the THz signal from the target. The power loss due to reflection is considered while estimating the imaging-related parameters of the radar, the details are described in the next section where the main interface of the tool is presented.

Fig. 3.28 shows the section of the QO channel interface that deals with the GRASP simulation. The interface is simple and convenient. The secondary fields are the given as the input to the GRASP simulation. The GRASP simulation yields the detector efficiency and the spillover efficiency of the dual Menlo lens system which can accessed in the Outputs section of the QO channel interface.

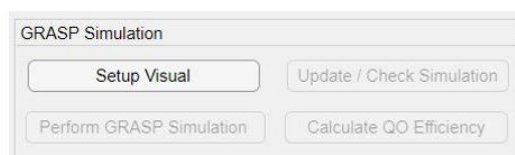


Figure 3.28: GRASP simulation section of the QO channel interface.

Fig. 3.29 shows the spillover efficiency of the dual Menlo lens system of the QO channel model and Fig. 3.30 shows the detection efficiency of the QO channel model receiver estimated using the GRASP simulation of the QO channel model with the Bow-tie antenna as the PCA. Fig. 3.31 shows the QO efficiency of the QO channel model. From Fig. 3.30, we can see that the horn antenna is a good receiver and the power loss in detection is much lower than the power loss at hemispherical lens. Similarly, Fig. 3.29 shows that the power loss due to the spillover in the QO path is also low as compared to the power loss at the hemispherical lens. Therefore, as mentioned before, the QO efficiency of the QO channel model with Bow-tie PCA is low because of the radiation efficiency of the hemispherical lens is low.

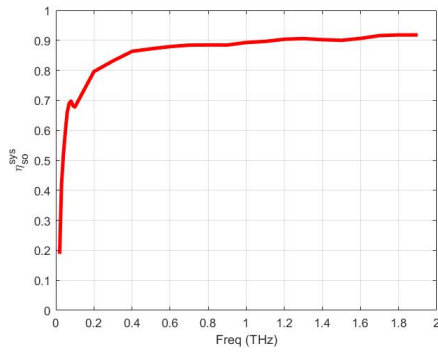


Figure 3.29: Spillover efficiency of the dual Menlo lens system in the QO channel model when the Bow-tie antenna is used as the PCA.

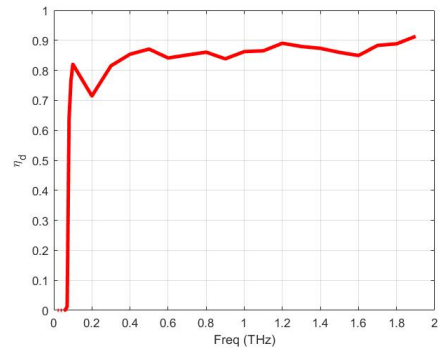


Figure 3.30: Detection efficiency of the QO channel model receiver when the Bow-tie antenna is used as the PCA.

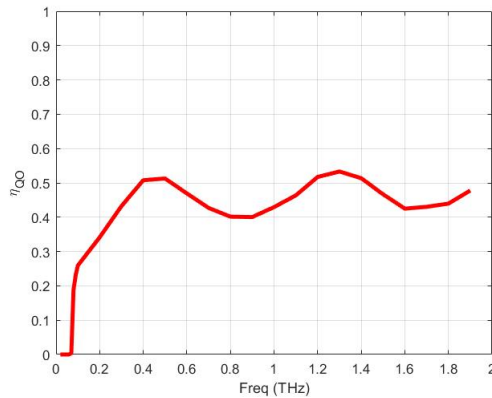


Figure 3.31: QO efficiency of the QO channel model when the Bow-tie antenna is used as the PCA.

QO channel model gives an insight into the power loss in the radar channel, however, it cannot be used as it is in the radar scenario to estimate the radar power loss. The reasons are: the radar scenario has the PCA at the reception whereas the QO channel model implements a horn antenna, the spillover due to distance between the target and the receiver and the power loss due to reflection from the target is not considered in the QO channel model. The hemispherical lens efficiency estimated in the QO channel model can be used on Tx and Rx side in the radar scenario as PCAs are used on the both Tx and Rx side in the scenario. The main interface considers the power loss due to reflection and the distance between the receiver and the target and estimates the total power loss in the radar channel which will be seen in the next section. Notably, we don't consider atmospheric path loss in the QO channel model as the distances we are working with in the QO channel model are very low and we can assume negligible atmospheric path loss over such distances.

Another important thing to take note is that the QO channel interface supports updating the parameters in the QO channel model in GRASP simulation, for example, the resolution of the GRASP simulation, the distance between different QO components etc. Fig. 3.32 shows the interface that updates the QO channel model parameters in the GRASP simulation. It can be

seen in the figure, that there are three types of parameters that can be updated, the first is the basic parameters, related to the resolution of the grid in the simulation and the shift of the receiver horn antenna from its default position in Fig. 2.4, etc. The second and third type of parameters are the component dimensions and component distances respectively.

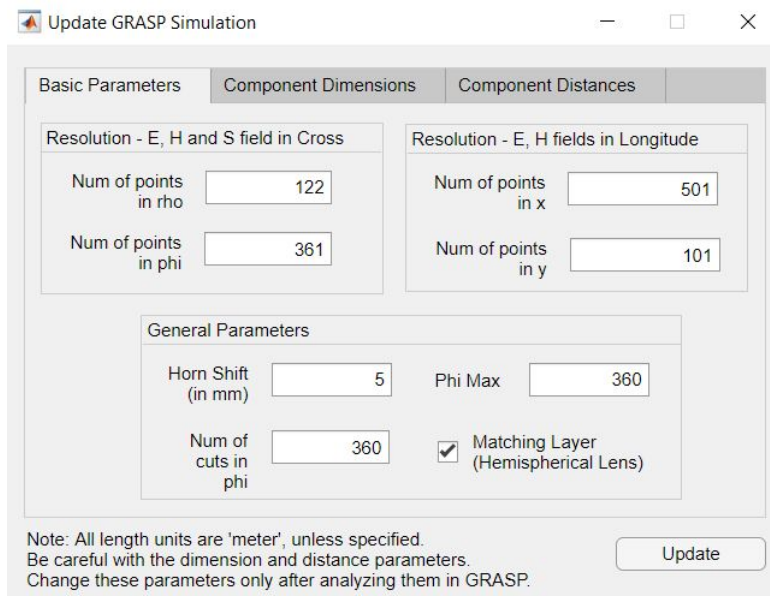


Figure 3.32: Interface to update the parameters related to the QO channel model, e.g., the resolution of the GRASP simulation, the distance between the QO-components, etc.

3.2.4 Outputs

Fig. 3.33 shows the section of the QO channel interface where the user can access the output efficiencies of different simulations we saw in the previous sections. In this section the user can plot the efficiencies or export the desired efficiency data to a Matlab data file.

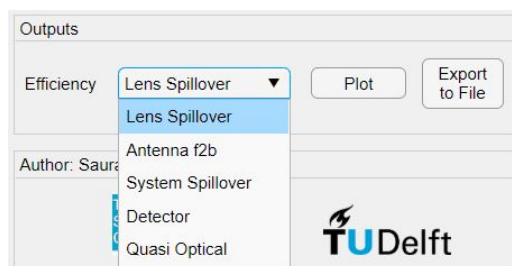


Figure 3.33: Outputs section of the QO channel interface.

3.3 Main Interface

We saw the transmitter interface and the QO channel interface of the tool in the previous sections. These interfaces estimate the power radiated by the PCAs in transmission and the power lost in the QO channel respectively. In this section, we will see the Main interface of the Matlab tool which performs the system dimensioning of the radar and estimates the imaging and detection parameters of the radar. The transmitter interface and the QO channel interface are accessed from the main interface and they assist the user to accurately estimate the imaging and detection parameters of the radar using the main interface. Fig. 3.34 shows the main interface of the Matlab tool. It can be seen in the figure that the interface is user-friendly. The radar scenario which is analyzed is clearly shown in the interface. The input and output parameters are separated by the dashed boxes in the figure. We will follow these dashed boxes to understand the utility of the main interface of the tool, however, before that it is important to visit the necessary theory behind the estimation of the imaging and detection parameters evaluated in the main interface.

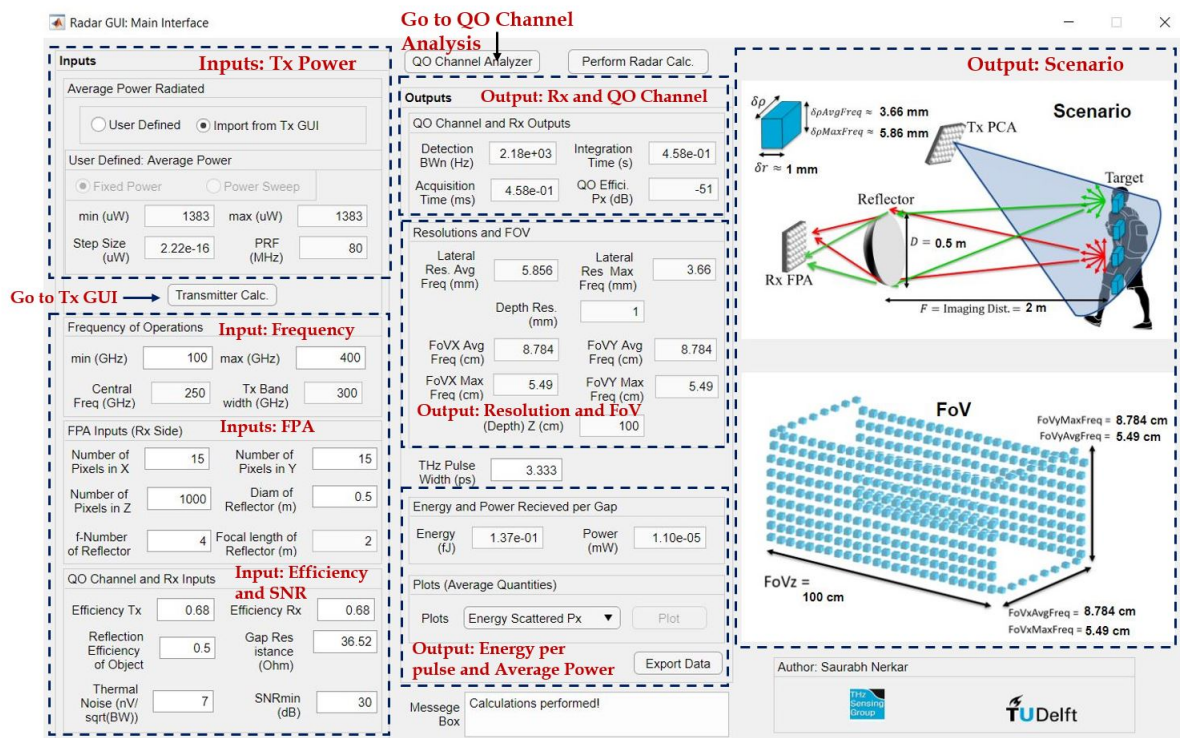


Figure 3.34: Main interface of the Matlab tool.

3.3.1 Theoretical background

In the last section, we learned that the QO channel model does not account for the power loss due to reflection of the THz power from the target and the power loss due to the spillover

of the signal because of the distance between the receiver and the target. In this section, we will see, how the main interface estimates the QO efficiency of the channel by considering the aforementioned losses. We will also see the theoretical calculations behind the imaging parameters such as the detection bandwidth, the integration time, the acquisition time, the field-of-view and the resolution of the radar.

3.3.1.1 Estimation of the channel loss

Fig. 3.35 shows the scenario used to calculate spillover efficiency of the QO path. The distance between the reflector and the target gives rise to the spillover of the power. This spillover has to be considered while calculating the QO efficiency. Spillover can be approximated by the following equation:

$$\eta_{so}^{sys} \approx \frac{\Omega_a}{\Omega_{pixel}} \quad (3.1)$$

where, Ω_a and Ω_{pixel} are the solid angles shown in the Fig. 3.35. Ω_{pixel} is the solid angle in which the target reflects the power which is 360° . Only the power reflected by a pixel in the solid angle that the pixel makes with the reflector is captured by the reflector, this solid angle is Ω_a .

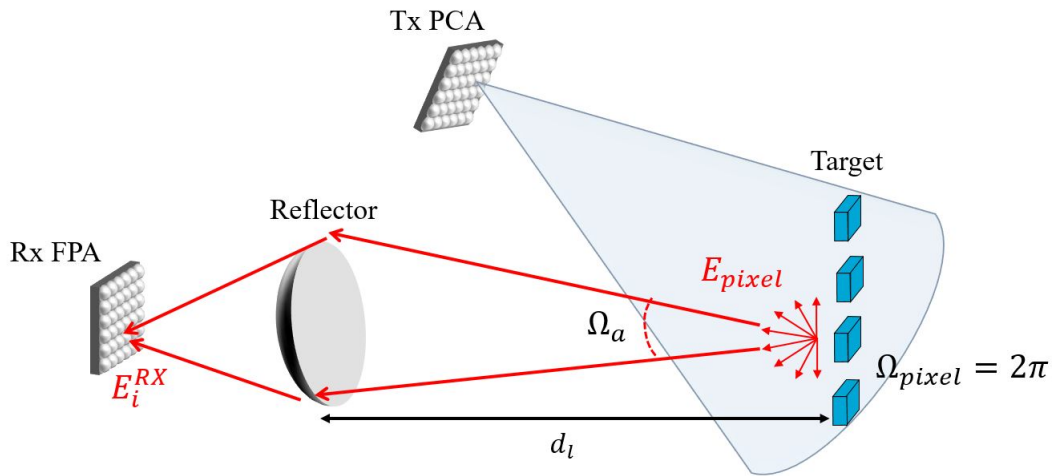


Figure 3.35: Scenario: Spillover calculations

Then, the QO channel efficiency per pixel of FPA utilizing the parameters specified in the Main interface with an assistance from the QO channel analyzer interface is calculated using the following expression:

$$\eta_{QO} = \frac{\eta_{Tx} * \eta_{Rx} * \eta_t * \eta_{so}^{sys}}{N_x * N_y} \quad (3.2)$$

where, η_{Tx} is the efficiency of the transmitter, η_{Rx} is the detection efficiency of the receiver, η_t is the target reflection efficiency and the N_x and N_y are the number of pixels/elements of FPA in x and y direction respectively.

Finally, the average energy, E_i^{Rx} received at each of the phototconductor gap of the Rx FPA is estimated using Eq. (2.30). And the average power received per FPA pixel is obtained from:

$$P_i^{Rx} = \frac{E_i^{Rx}}{PRF} \quad (3.3)$$

Fig. 3.36 shows the QO efficiency of the path as a function of the distance between the reflector and the target, i.e. as a function of the spillover, assuming $\eta_{Tx} = \eta_{Rx} = 0.68$ obtained from the QO channel interface for the Bow-tie PCA model, $\eta_t = 0.5$ and $N_x = N_y = 15$. It can be seen from the figure that as the distance increases, the QO efficiency decreases.

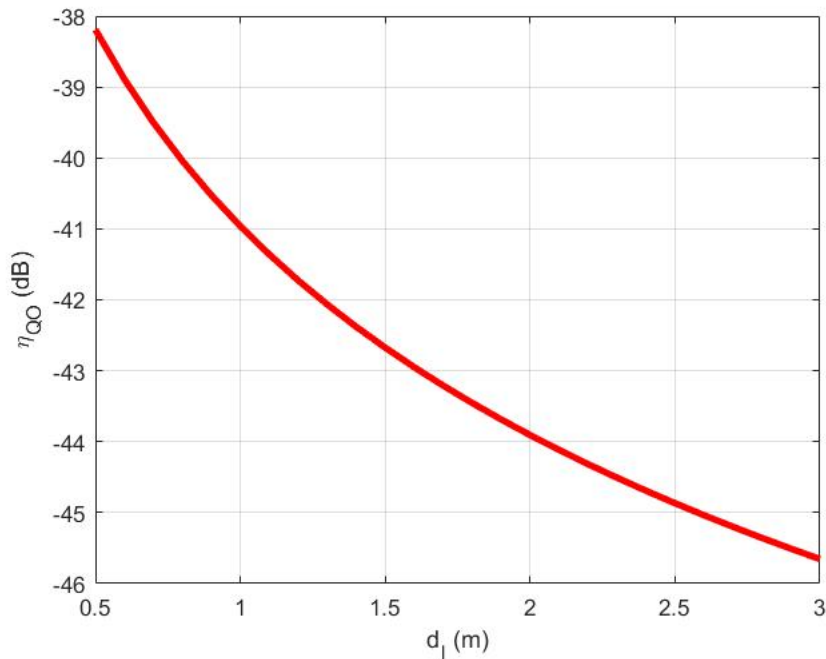


Figure 3.36: η_{QO} as a function of the distance between the reflector and the target.

3.3.1.2 Detection Bandwidth

Let's derive the detection bandwidth. First let's assume average energy reaching each receiver gap is E_i^{Rx} . Then, the power per pulse reaching each gap is defined as $P_{\tau,i}^{Rx}$ and is given by below equation:

$$P_{\tau,i}^{Rx} = \frac{E_i^{Rx}}{\tau_p} \quad (3.4)$$

where, τ_p is the pulse width of the THz signal. The power per pulse reaching each gap can also be given by,

$$P_{\tau,i}^{Rx} = \frac{v_{\tau,i}^2}{R_g} \quad (3.5)$$

where, $v_{\tau,i}$ is the voltage generated in the PCA gap after a THz wave impinges on the PCA. R_g is the semiconductor gap resistance. Power received is calculated based on the calculations in

equation (3.4) and the efficiency calculations seen in the previous part of the section.

Once the voltage induced in the semiconductor gap is calculated, average voltage is expressed as:

$$v_{avg} = v_{\tau,i} \frac{\tau_{\tau,i}}{T_i} \quad (3.6)$$

where, $\tau_{\tau,i}$ is the pulse width of the THz wave and T_i is the pulse repetition time of the same. The pulse width of the THz wave is estimated using the following relation:

$$\tau = \frac{1}{BW_{Pulse}} \quad (3.7)$$

where, BW_{Pulse} is the pulse bandwidth.

Based on the parameters calculated so far the SNR of the system can be estimated as:

$$SNR = \frac{v_{gap}}{\langle v_n \rangle} = \frac{\text{average signal induced at each Rx Gap}}{\text{average noise voltage}} \quad (3.8)$$

From the above relations average noise voltage, $\langle v_n \rangle$, can be estimated. Then, the detection bandwidth, BW_n , can be estimated from the following relation:

$$BW_n = \left(\frac{\langle v_n \rangle}{s_{v,n}} \right)^2 \quad (3.9)$$

where, $\langle s_{v,n} \rangle$ is the Johnson (Thermal) noise level. It is estimated to be $7nV/\sqrt{Hz}$ for commercially available Menlo THz time-domain system.

3.3.1.3 Acquisition Time

Acquisition time is the time required by the system to image (acquire) a single point of the target within the possible range. Based on the detection bandwidth, BW_n , of a radar, the acquisition time can be estimated with the following relation:

$$T_{acq} = \frac{1}{BW_n} \quad (3.10)$$

3.3.1.4 Integration Time

The integration time is the time taken by the radar system to acquire/image all the points in its field of view or to obtain the a trace. The integration time is estimated using the following relation:

$$T_{integration} = T_{acq} * N_z \quad (3.11)$$

where, N_z is the number of pixels in the radar range.

3.3.1.5 FoV and Radar Resolution

It is established before that in the radar scenario, depicted in Fig. 1.1 a focal plane array with number of elements N_x in \hat{x} and number of elements N_y in \hat{y} is used to receive the signal reflected from the target. Therefore, number of pixels in the direction x and y are N_x and N_y respectively. Number of pixels in range are defined as N_z . Then, the Field of View (FoV) of the radar is obtained using following expression:

$$FoV_p = N_p * Resolution \text{ in } P \quad (3.12)$$

where, FoV_p is the FoV in any direction \hat{p} , N_p , is the number of pixels in the direction \hat{p} .

Lateral resolution of the radar is given as below:

$$\delta_p = \frac{1.22 * N_f * c}{freq} \quad (3.13)$$

where, N_f is the f-number of the reflector, c is the speed of light and $freq$ is the frequency of operation of the radar. Eq. (3.13) calculates the lateral resolution of a QO reflector. It should be noted that the radar scenario presented in the Fig. 1.1 uses a reflector to focus the radiation reflected from the target, however, it can be replaced with other QO-components provided the propagation mechanism remains the same, this is already explained in chapter 2. In future if a different QO component such as a hyperbolic lens is used in the radar scenario, the relation given in Eq. (3.13) has to be changed accordingly.

Range resolution is evaluated using the following equation:

$$Range \text{ Resolution} = \frac{c}{BW_{Tx}} \quad (3.14)$$

where, c is the speed of light and BW_{Tx} is the bandwidth of the THz signal.

In this part of the section, we have covered the necessary theoretical background behind the imaging and detection parameters estimated by the main interface of the Matlab tool. Next part onward, we will see the different input and output sections of the main interface and understand the utility of the interface.

3.3.2 Input: Power Radiated by Tx

Fig. 3.37 shows the section of the main interface that deals with the power radiated by the transmitter. Power radiated by the transmitter is an input parameter for the radar imaging and detection analysis. The input power can be specified using two options:

1. "User Defined Inputs": desired values of power can be inputted in unit micro-watts (μW).

This option is handy when an approximate radar design is expected and approximate power radiated values are known.

- "Import from the Tx GUI": this option invokes the transmitter interface of the Matlab tool where the Norton equivalent circuit of the PCAs is implemented and accurate values of the power radiated by the given array of PCAs is estimated. The values calculated are then exported to the main interface for further analysis. In Fig. 3.37 we use the bow-tie connected array configuration mentioned in Section 3.1.

Figure 3.37: Input section of the main interface where the power radiated by the transmitter PCA is specified.

The inputs expected by this section of the main interface are: range in which the power radiated by the Tx varies, minimum, maximum and step size is required, and the PRF of the THz signal. The units of the parameters are mentioned in Fig. 3.37. In case of option "Import from the Tx" is chosen, all these fields will be automatically populated by the values exported by the transmitter interface of the Matlab tool. The values in the figure, are imported from the Tx interface and evaluated for the Bow-tie antenna PCA as specified in Section 3.1.

3.3.3 Input: Frequency of Operation and FPA Details

Fig. 3.38 shows the section of the main interface that expects the "Frequency of Operation and FPA details" as inputs.

Figure 3.38: Section of the main interface where frequency of operation of the radar and the FPA details should be provided.

The first set of inputs is the frequency band of operation i.e. the frequency band of radiated THz signal. It can be specified from a minimum to a maximum value. The central frequency and

the signal bandwidth are calculated automatically by the tool. The unit of the set of frequency variables in this section is GHz. For the Bow-tie antenna the frequency band of operation is 100 GHz - 400 GHz.

The next set of inputs is the Rx Focal Plane Array (FPA) details, values of the following parameters are expected as inputs:

- number of pixels in x and y which are the number of elements in x and y in a $N_x \times N_y$ FPA of PCAs
- number of pixels in z which is the number of pixels expected in the range trace e.g. if the range resolution of the radar is 1 mm, and the desired trace is 1 m, then the number of pixels in range (z) 1 m is 1000
- diameter of the reflector antenna which is used as a QO component to focus the THz signal reflected from the target on to the receiver FPA.
- f-Number of reflector of the aforementioned reflector antenna.

These inputs together describe the frequency and the Rx side of the scenario. it should be noted that the imaging distance in Fig. 1.1 is the distance between the target and the reflector. It is taken to be same as that of the focal length of the reflector.

Fig. 3.38 shows the example frequency and Rx FPA input parameters that belong the the radar scenario depicted in 1.1 with a Bow-tie as a PCA as mentioned in Section 3.1. Table 3.3 summarizes these input parameters.

Table 3.3: Summary of the frequency of operation and Rx FPA details specified for the radar design using Bow-tie PCA.

Parameter	Value
Min frequency of operation	100 GHz
Max frequency of operation	400 GHz
Central frequency of operation	250 GHz
Tx bandwidth	300 GHz
Number of pixels in FPA in X	15
Number of pixels in FPA in Y	15
Expected number of pixels in range i.e. Z	1000
Diameter of the reflector	0.5 m
f-number of the reflector	4
Focal length of the reflector	2

3.3.4 Input: QO Channel and Rx Inputs

Fig. 3.39 shows the section of the main interface of the Matlab tool describing the QO channel and receiver inputs.

QO Channel and Rx Inputs			
Efficiency Tx	0.68	Efficiency Rx	0.68
Reflection Efficiency of Object	0.5	Gap Resistance (Ohm)	36.52
Thermal Noise (nV/sqrt(BW))	7	SNRmin (dB)	30

Figure 3.39: Section of the main interface where the QO channel efficiencies and the desired Rx parameters such as the SNR are specified.

The fields in this section are divided into two parts: QO Channel inputs and receiver side inputs.

3.3.4.1 QO channel Inputs

Following parameters are taken as the QO channel inputs:

- efficiency of the transmitter, η_{Tx} , which quantifies the power loss in the PCA transmitter
- efficiency of the receiver, η_{Rx} which quantifies the power loss in the reception of the signal
- reflection efficiency of the target, η_t which is a measure of the power loss due to the reflection of the THz signal from the target.

As seen previously, the QO channel interface can assist the user in determining the aforementioned efficiencies. We have seen in Section 3.2 that the QO channel model is not entirely similar to the radar scenario. However, as the radar scenario utilizes the PCA array at both receiver and transmitter, the transmitter and receiver efficiencies can be assumed reasonably similar to the radiation efficiency of the hemispherical lens, η_{rad}^l , which is coupled with the PCA. Therefore, the transmitter and receiver efficiencies can be given as:

$$\eta_{Tx} = \eta_{Rx} = \eta_{rad}^l \quad (3.15)$$

The spillover efficiency of the radar scenario system, η_{so}^{sys} and the QO channel efficiency of the radar scenario η_{QO} are estimated as described in the Section 3.3.1.1, in these calculations the users can assume a value for the reflection efficiency of the target, η_t . In our case, we assume $\eta_t = 0.5$. The average energy and power received per pixel of the FPA is evaluated from the η_{QO} as described in the Section 3.3.1.1.

The efficiencies mentioned in Fig. 3.39 belong to the QO channel model with the Bow-tie antenna described previously in the chapter as the PCA.

3.3.4.2 Rx Inputs

Rx inputs expected in the Fig. 3.39 are:

- gap resistance, R_g of the PCA unit in the FPA
- thermal noise level in the receiver, $\langle s_{v,n} \rangle$
- minimum signal-to-noise ratio expected, SNR.

We have seen in section 2.1 that the Norton equivalent circuit of the PCA estimates the gap resistance of the PCA using the Eq. (2.8). The users can take assistance from the transmitter interface to estimate this parameter, as the PCAs on the Rx side can be similar to the PCAs on the Tx side. For example, the value of the gap resistance specified in the Fig. 3.39 belongs to the Bow-tie PCA previously described in the chapter and estimated using the transmitter interface. We have seen the gap resistance as a function of the input laser power in Fig. 3.11.

The values of the different parameters shown in Fig. 3.39 belong to the QO channel model with the Bow-tie as the PCA, as mentioned before. Other parameters are desired design parameters for the radar scenario shown in Fig. 1.1. Table 3.4 summarizes the values of the QO channel and Rx inputs specified as an example to understand the utility of the tool.

Table 3.4: Input parameter values for section, QO channel and Rx inputs

Parameter	Value
η_{Tx}	0.68
η_{Rx}	0.68
η_t	50 %
R_g	36.52 Ω
Thermal Noise	$7 \text{ nV} / \sqrt{BW}$
Minimum expected SNR	30 dB

Inputs of the Matlab tool's main interface are discussed as above, now let's look at its outputs.

3.3.5 Output: QO Channel and Rx Outputs

This section shows the imaging parameters of the radar viz., the detection bandwidth, BW_n , the integration time, T_{int} and the acquisition time, T_{acq} and the QO channel efficiency, η_{QO} evaluated by the main interface of the Matlab tool using the input parameters given by the users and described in the previous sections. These parameters are defined in detail in Section 3.3.1.

Fig. 3.40 shows section of main interface which displays the QO channel efficiency and imaging parameters as outputs.

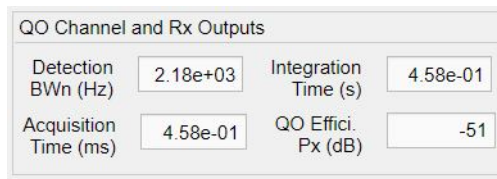


Figure 3.40: Section of the main interface of the Matlab tool which displays the QO channel and imaging parameters.

Table 3.5 gives the summary of the imaging parameters and the QO efficiency results obtained when the Bow-tie antenna described previously is used as a PCA in the QO channel model.

Table 3.5: Summary of the QO channel and Rx outputs when a Bow-tie is used as a PCA in the QO channel model.

Parameter	Value
Detection BW	2.18 kHz μW
Integration time	0.458 s
Acquisition time	0.458 ms
QO efficiency per FPA pixel	-51 dB

Fig. 3.41, Fig. 3.42 and Fig. 3.43 show the integration time, acquisition time and the detection bandwidth of the radar as a function of the power radiated by the Tx respectively. It can be seen that, as the power radiated increases, the integration time and acquisition time decreases. The detection bandwidth is directly proportional to the power radiated by the Tx and it increases with the increase in the power radiated by the transmitter. Conclusion, it is better to have a transmitter that can radiate the more. All the parameters apart from the power radiated by the Tx, discussed in the above sections, were kept constant to get this parametric analysis.

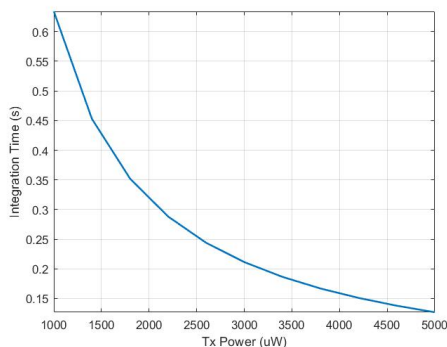


Figure 3.41: Integration time of the radar as a function of the power radiated by the Tx.

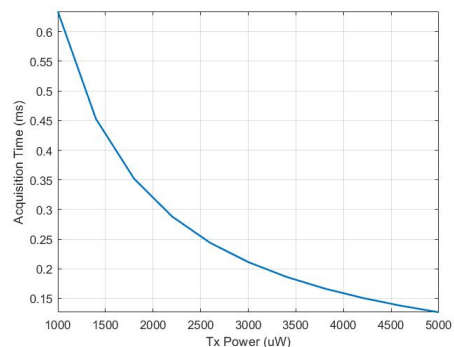


Figure 3.42: Acquisition time of the radar as a function of the power radiated by the Tx.

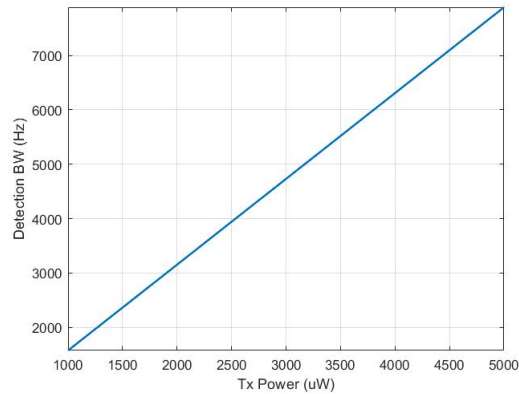


Figure 3.43: Detection bandwidth of the radar as a function of the power radiated by the Tx.

3.3.6 Output: Resolutions and FoV

Resolution and the FoV of the radar are the most important imaging parameters. These parameters are necessary to understand how the radar design is behaving and how the design will have advantages over the other similar designs. The theory behind these parameters is discussed in Section 3.3.1. In this section, the part of the main interface which outputs the resolution and FoV of the radar is discussed.

Fig. 3.44 shows the section of the Matlab tool's main interface which presents the Resolutions and Field of View (FoV) outputs.

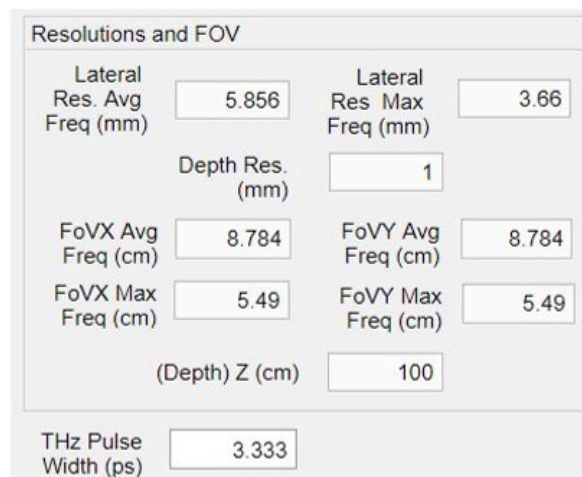


Figure 3.44: Section of the main interface of the Matlab tool that displays the resolution and the FoV of the radar.

The resolution and radars parameters estimated by the main interface are: the lateral resolution of the radar at central and maximum frequency of operation, the depth resolution of the radar, the FoV of the radar in \hat{x} and \hat{y} direction at the central and maximum frequency of operation, and finally, the depth/FoV in range of the radar i.e. the range trace of the radar. The units of these parameters can be seen in Fig. 3.44. It can be seen in Fig. 3.34 that the FoV of the radar and the radar scenario are visualized in the main interface of the Matlab tool for the

better understanding of these parameters. Fig. 3.45 shows this FoV.

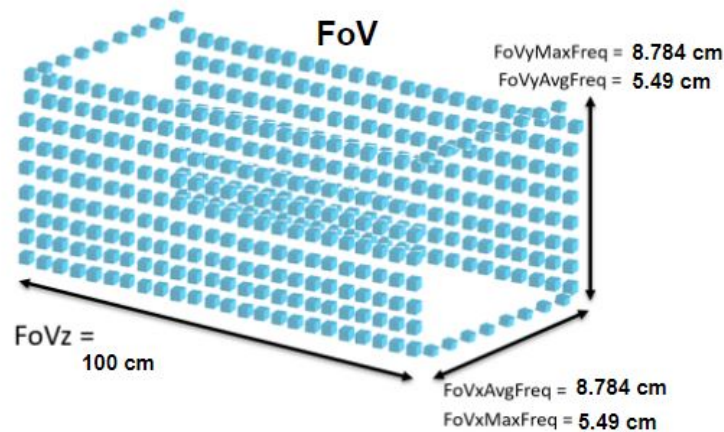


Figure 3.45: FoV of the radar with input parameters as shown in Fig. 3.34.

3.3.7 Output: Energy and Power Received per Gap

Fig. 3.46 shows the section of the tool's main interface which presents the output values "Energy and Power Received per Gap".

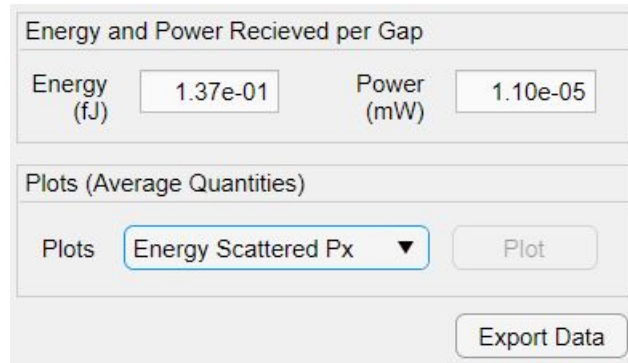


Figure 3.46: Section of the main interface that displays the energy and power received at a single PCA gap of the FPA.

The outputs presented in this section are: the average energy and the average power received at the gap of the each of the FPA element. The energy is specified in femto-Joule and the power is specified in milli-Watts.

It can be noted that the plot section which can be seen in Fig. 3.46 facilitates the visual representation of the variation in the parameters such as the energy received, power received or the other radar parameters such as the detection bandwidth with respect to the variation in the power transmitted, if the transmitted power sweep is provided as input.

When a Bow-tie antenna is used as the PCA with the input parameters described in the previous sections, 0.139 fJ of the average energy and 11.1 nW of average power is received in the gap of a single PCA in the FPA.

Fig. 3.47 and 3.48 represent the energy and power received at the gap of a single PCA in the

FPA as a function of the power radiated by the Tx respectively. The variation is linear owing according to the Eq. (2.30). If the the power radiated by the transmitter is higher, the power received at the FPA will be higher and the SNR will be better.

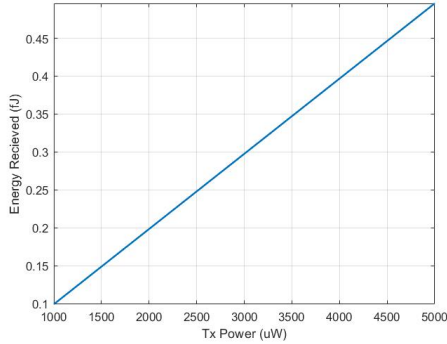


Figure 3.47: Energy received at the gap of a single PCA in the FPA as a function of the power radiated by the Tx.

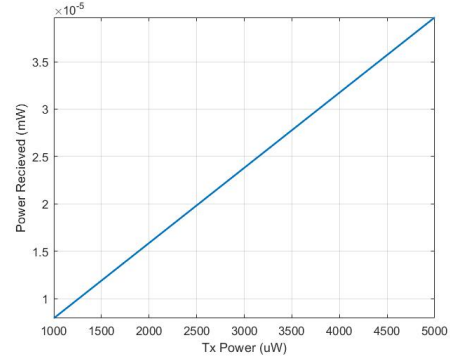


Figure 3.48: Power received at the gap of a single PCA in the FPA as a function of the power radiated by the Tx.

3.3.8 Conclusion

We saw the transmitter interface, the QO channel interface and the main interface of the Matlab tool in the previous sections. The interdependence of the multiple parameters involved was also studied using the parametric analyses over the parameters. In particular, when we choose the input parameters as described in the Table 3.6, we can achieve a radar design with approximate FoV $6cm \times 6cm \times 100cm$, lateral resolution of around $4mm$ and range resolution of $1mm$.

Table 3.6 summarizes the values of the important input parameters used to achieve the aforementioned radar design. As mentioned before, these parameters belong to the setup where Bow-tie is used as a PCA. Table 3.7 summarizes the obtained output parameters.

Table 3.6: Inputs provided to the main interface of the Matlab tool to evaluate the radar scenario with Bow-tie as a PCA

Input Parameter	Value
Transmitted Power	1.383 mW
THz signal PRF	80 MHz
Transmitted bandwidth	300 GHz
Number of elements of FPA	225
Minimum SNR	30 dB
Reflector Diameter	0.5 m
F-number of reflector	4
Tx Efficiency	0.68
Rx Efficiency	0.68
Target reflection efficiency	0.5
Gap resistance	36.52 Ω

Table 3.7: Example outputs of the main interface of the Matlab tool

Output Parameter	Value
Detection BW	2.18 kHz
Acquisition time	0.458 <i>ms</i>
Integration time	0.458 s
Lateral resolution	3.66 mm
Depth resolution	1 mm
FoV in X, FoV in Y	5.49 cm
Range trace	100 cm
Average energy reaching Rx	0.137 <i>fJ</i>
Average power reaching Rx	11.0 <i>nW</i>

The technology of THz time-domain radars is changing rapidly as numerous researches around the globe are working constantly to improve the utility and usability of these radar systems. Considering this, the Matlab tool is developed in such a manner that it is easily expandable and can be swiftly updated to accommodate any future amendments in the PCA, QO channel or radar model to improve its functionality along with its accuracy and reliability.

Chapter 4

Conclusion

4.1 Summary and Conclusion

The applications of the THz technology are growing rapidly, the main reason behind this is the wide available bandwidth in the THz domain. One of the prominent applications of THz technology is the THz time-domain radar. The THz time-domain radars can achieve a field of view comparable to the current state-of-the-art sub-mm security standoff radars with better resolution. THz time-domain radars will be the next ground-breaking technology in the domain of public safety and security. The variety of applications of the THz technology are driven by Photoconductive Antennas (PCAs). PCAs can generate THz signals with bandwidth up to a few THz and at a relatively low cost.

The THz time-domain radar design has three main aspects: the transmitter design, the QO channel analysis and the radar receiver design. The main aspect of the transmitter design is that it should produce THz power at least of the order of mW for the radar to work properly. The power loss in the propagation of the THz signal from the transmitter to the receiver of the radar is estimated from the QO path analysis. Finally, principles of detection and imaging are used to estimate the radar parameters such as the received power and energy, the field of view and the resolution of the radar.

Design and analysis of each of the parts of the THz time-domain radar system are in itself intense, time-consuming and requires knowledge of multiple subjects which might not be the area of expertise of a radar engineer. Therefore, the process of designing and analysing a complete THz time-domain radar is a challenging task even for a preliminary design at a top-level. This thesis attempts to solve difficulties in the THz time-domain radar design by introducing a Matlab Graphical User Interface (GUI) for system dimensioning and QO channel analysis of the radar. The developed Matlab tool allows people to design their desired THz radar system without knowing the fundamentals. The main objectives fulfilled by the Matlab tool are: to estimate the power radiated by the PCA transmitter, to estimate the power loss in the QO chan-

nel model and the power received at the receiver and to design and analyze a THz radar for high-resolution security application at a preliminary level.

The Matlab tool is divided into three parts: the transmitter interface, the QO channel interface and the main interface. The transmitter interface of the tool implements the Norton equivalent circuit of the PCAs to estimate the power radiated by the PCA on the transmitter side. The QO channel interface of the tool implements a QO channel model that has a similar propagation mechanism as that of the THz radar and using this model, the tool estimates the QO channel efficiency which characterizes the power loss in the QO channel and the power received at the receiver. The models implemented in the tool and their theoretical background was discussed in chapter 2. Finally, the main interface of the tool implements the detection and imaging principles to estimate the imaging parameters of the radar such as the resolution and the field of view.

Chapter 3 of the thesis, describes the GUI of the tool in detail. First, the transmitter interface of the tool was introduced. The Norton equivalent circuit of the Bow-tie PCA was analyzed in the transmitter interface to present the utility of the tool. The interdependence of multiple parameters was studied and analyzed. Then, the QO channel interface was explained. The utility of the interface was presented by using a Bow-tie PCA in the QO channel model. Different sections of the QO channel models cater to different simulations performed in the QO channel interface. These simulations were performed on the model with Bow-tie as PCA and the results were presented. Lastly, the main interface of the tool was presented. Various inputs and outputs of the main interface and the utility of the interface were explained using the Bow-tie antenna as a PCA. The transmitter interface and the QO channel interface can be accessed through the main interface of the tool. The transmitter interface quantifies the THz power radiated by the PCAs, the QO channel interface assists the users in estimating the power loss in the channel by analyzing the QO channel model and finally, the main interface of the Matlab tool performs the system dimensioning of the THz time-domain radar considered in the thesis work.

It can be noted about the Matlab tool that it is developed in such a manner that it is easily expandable and can be swiftly updated to accommodate any future amendments in the PCA, QO channel or radar model to improve its functionality along with its accuracy and reliability.

4.2 Future Work

This project implemented the Norton Equivalent circuit of the PCAs, the QO channel model and also the imaging and detection parameter estimation for a high-resolution security imaging application. The Matlab tool that has been developed helps one to design radar for this specific application with ease. However, there is a lot of scope for improvement and further research and development.

The first important aspect to be considered for improvement is the implementation of the transmitter. As seen in the previous chapters, the tool implements the circuit developed in [20]. However, there have been recent developments [27] in the field. The equations are now being improved to be more accurate. Better formulae will be implemented in future for obtaining accurate results. The advantage of the Matlab tool is that it is expandable and can accommodate the changes in the formulae.

Another limitation of the tool is that it does not implement the connected array of the PCAs, instead, it linearly evaluates the power for the set of PCAs. This can be improved in the future by implementing an actual connected array circuitry in the transmitter interface of the tool.

On the QO channel model part also as the research progresses, better channel models can be implemented in future. These models will take as few inputs as possible and simulate the QO channel as accurate as possible. Apart from the accuracy of the model, the time it takes for PO in Tx simulation and the QO simulation of the QO channel model can also be improved in the future.

The current tool does not have circuitry on the receiver side. Currently, it considers an FPA at the reception and based on received power, it estimates the quantities such as the SNR and the integration time of the radar. This can be improved in future by adding complete receiver-side calculations to the tool.

Bibliography

- [1] R. Appleby and H. Wallace, “Standoff detection of weapons and contraband in the 100 GHz to 1 THz region,” *IEEE Transactions on Antennas and Propagation*, vol. 55, no. 11, pp. 2944–2956, 2007.
- [2] K. Cooper, R. Dengler, N. Llombart, B. Thomas, G. Chattopadhyay, and P. Siegel, “THz imaging radar for standoff personnel screening,” *IEEE Transactions on Terahertz Science and Technology*, vol. 1, no. 1, pp. 169–182, 2011.
- [3] L. Zanutto, R. Piccoli, J. Dong, D. Caraffini, R. Morandotti, and L. Razzari, “Time-domain terahertz compressive imaging,” *Opt. Express*, vol. 28, pp. 3795–3802, Feb 2020.
- [4] B. M. Fischer, H. Helm, and P. U. Jepsen, “Chemical recognition with broadband thz spectroscopy,” *Proceedings of the IEEE*, vol. 95, no. 8, pp. 1592–1604, 2007.
- [5] X. Yang, X. Zhao, K. Yang, Y. Liu, Y. Liu, W. Fu, and Y. Luo, “Biomedical applications of terahertz spectroscopy and imaging,” *Trends in Biotechnology*, vol. 34, no. 10, pp. 810–824, 2016.
- [6] P. Jepsen, R. Jacobsen, and S. Keiding, “Generation and detection of terahertz pulses from biased semiconductor antennas,” *J. Opt. Soc. Am. B*, vol. 13, no. 11, p. 2424–2436, 1996.
- [7] S. Preu, S. Dhler, G.H. andMalzer, L. Wang, and A. Gossard, “Tunable, continuous-wave terahertz photomixer sources and applications,” *J. Appl. Phys.*, vol. 109, 061301, 2011.
- [8] M. Tani, S. Matsuura, K. Sakai, and S. Nakashima, “Emission characteristics of photoconductive antennas based on low-temperature-grown GaAs and semi-insulating GaAs,” *Appl. Opt.*, vol. 36, no. 30, p. 7853–7859, 1997.
- [9] E. R. Brown, “Thz generation by photomixing in ultrafast photoconductors,” *Int. J. High Speed Electron. Syst.*, vol. 13, no. 2, pp. 497–545, 2003.
- [10] G. Loata, M. Thomson, T. Loffler, and H. Rokos, “Radiation field screening in photoconductive antennae studied via pulsed terahertz emission spectroscopy,” *App. Phys. Lett.*, vol. 91, p. 232506, 2007.
- [11] H. Roehle, R. J. B. Dietz, H. J. Hensel, J. Bttcher, H. Knzel, D. Stanze, M. Schell, and B. Sartorius, “Next generation 1.5 μm terahertz antennas: mesa-structuring of InGaAs/InAlAs photoconductive layers,” *Opt. Exp.*, vol. 18, pp. 2296–2301, 2010.

- [12] C. Berry and M. Jarrahi, "Principles of impedance matching in photoconductive antennas," *J. Infrared Milli. Terahz. Waves*, vol. 33, no. 12, pp. 1182–1189, 2012.
- [13] N. Khiabani, Y. Huang, Y. Shen, and S. Boyes, "Theoretical modelling of a photoconductive antenna in a terahertz pulsed system," *IEEE Trans. Antennas Propag.*, vol. 61, no. 4, pp. 1538–1546, 2013.
- [14] S. Peru, "A unified derivation of the Terahertz spectra generated by photoconductors and diodes," *J. Infrared Milli. Terahz. Waves*, vol. 35, no. 12, pp. 998–1010, 2014.
- [15] R. Emadi, N. Barani, R. Safian, and A. Zeidaabadi Nezhad, "Hybrid computational simulation and study of Terahertz pulsed photoconductive antennas," *J. Infrared Milli. Terahz. Waves*, vol. 37, no. 11, pp. 1069–1085, 2016.
- [16] A. Garufo, P. M. Sberna, G. Carluccio, J. R. Freeman, D. R. Bacon, L. Li, J. J. Baselmans, E. H. Linfield, A. G. Davies, N. Llombart, and et al., "A connected array of coherent photoconductive pulsed sources to generate mW average power in the sub-millimeter wavelength band," *IEEE Transactions ON Terahertz Science And Technology*, vol. 9, no. 3, 2018.
- [17] S. Orfanidis, "Electromagnetic Waves and Antennas." <http://www.ece.rutgers.edu/orfanidi/ewa/>, 2013.
- [18] A. Pelekanidis, "A THz lens antenna fed by a photoconductive connected dipole array," Master's thesis, Delft University of Technology, the Netherlands, 2020.
- [19] O. Castañeda-Uribe, C. Criollo, S. Winnerl, M. Helm, and A. Avila, "Comparative study of equivalent circuit models for photoconductive antennas," *Opt. Express*, vol. 26, pp. 29017–29031, 2018.
- [20] A. Garufo, G. Carluccio, N. Llombart, and A. Neto, "Norton equivalent circuit model for pulsed photoconductive antennas - part I: Theoretical model," *IEEE Transactions on Antennas and Propagation*, vol. 66, no. 4, 2018.
- [21] A. Garufo, G. Carluccio, J. R. Freeman, D. R. Bacon, N. Llombart, E. H. Linfield, A. G. Davies, and A. Neto, "Norton equivalent circuit model for pulsed photoconductive antennas - part II: Experimental validation," *IEEE Transactions on Antennas and Propagation*, vol. 66, no. 4, 2018.
- [22] Ticra, "TICRA Tools 19.1.1 - GRASP." <https://www.ticra.com/>, 2019.
- [23] Dassault Systems, "CST Studio Suite 2018." <https://www.3ds.com/products-services/simulia/products/cst-studio-suite/solvers/>, 2018.
- [24] D. Filipovic, S. Gearhart, and G. Rebeiz, "Double-slot antennas on extended hemispherical and elliptical silicon dielectric lenses," *IEEE Transactions on microwave theory and techniques*, vol. 41, no. 10, pp. 1738–1749, 1993.
- [25] H. Zhang, "A GO/FO tool for analyzing Quasi-optical systems in reception," Master's

- thesis, Delft University of Technology, the Netherlands, 2018.
- [26] A. Ludwig, “The definition of cross polarization,” *IEEE Transactions on Antennas and Propagation*, vol. 21, no. 1, pp. 116–119, 1973.
- [27] A. Bernardis *et al.*, “On the accurate characterization of pulsed photoconductive sources: Theory vs measurements,” *EuCAP*, 2021.
- [28] A. Garufo, *Towards the engineering of pulsed photoconductive antennas*. PhD thesis, Delft University of Technology, 2017.

Appendix A

Laser Model and Laser GUI

A.1 Laser Model

Laser source is used to generate electron-hole pairs in photoconductor. This laser source is characterized by a spectral band centered around a laser carrier frequency. [20]

Gaussian time envelope of the laser is defined as in equation (A.1)

$$\tilde{s}_n(t) = e^{-4\ln 2 \left(\frac{t}{\tau_p}\right)^2} \quad (\text{A.1})$$

Gaussian spatial distribution is given by equation (A.2)

$$|\tilde{s}_n(\rho, z = 0)| = e^{-4\ln 2 \left(\frac{\rho}{D_{-3dB}}\right)^2} \quad (\text{A.2})$$

This source is a paraxial wave modulated by a slow varying pulses, therefore, $B_{laser} \ll f_{laser}$ [20]

The electric field of the laser beam is given by equation (A.3).

$$e_{laser}(r; t) = e_{laser}(\rho, z) f\left(t - \frac{z}{c}\right) \sin(\omega_{laser} t - k_{laser} z + \phi_{laser}) \quad (\text{A.3})$$

In above equation, *sin* term is the carrier signal, *f* term is the modulating signal and $e_{laser}(\rho, z)$ is the spatial distribution of the electric field.

Modulating signal f is defined by equation (A.1).

Now, the area of laser beam is defined as below:

$$A_{laser}(z) = \int_{-\infty}^{\infty} \int_{-\infty}^{\infty} \tilde{s}_n(\rho, z) \cdot \hat{z} dx dy \quad (A.4)$$

Then these equations lead to peak values of pulse power, power spectral density, pulse energy and electric field as below:

$$Peak\ Pulse\ Power = P_0 = P_{laser} \frac{T_p}{\tau_p} \sqrt{\frac{4 \ln(2)}{\pi}} \quad (A.5)$$

$$Power\ Density\ Peak = S_0 = \frac{P_0}{A_{laser}} \quad (A.6)$$

$$Peak\ Pulse\ Energy = E_p = P_{laser} * T_p \quad (A.7)$$

$$Electric\ Field\ Peak = E_0 = \sqrt{S_0 * 2\eta_d} \quad (A.8)$$

In above equations, T_p is the pulse repetition time of the laser, τ_p is the pulse width of the laser and η_d is the characteristic impedance of the semiconductor material.

Another important factor in the laser model is the spillover of the laser power. When the area of the laser beam is larger than the area of the semiconductor gap some of the laser power is lost to the atmosphere. Spillover efficiency of the laser is the measure of this power loss, it is expressed as below:

$$\eta_{spillover}^{laser} = \frac{W_x * W_y}{A_{laser}} \quad (A.9)$$

where, W_x and W_y are the width and the length of the PCA semiconductor gap respectively, and the A_{laser} is the area of the laser beam as defined in Eq. (A.4).

A.2 Laser GUI

Laser GUI has been implemented to calculate the parameters seen in the previous section. This GUI gives an insight into how exactly the laser is characterized by providing necessary peak values of the output EM wave of the laser source. Apart from that the GUI visualizes the spatial distribution of the electric field and the power spectral density of the laser source. The GUI is simple to use and it is a part of the "Transmitter Window" of the "Radar GUI".

Figure A.1 shows Laser GUI. This GUI can be accessed by pressing Transmitter Window's "Analyze Laser Beam" button.

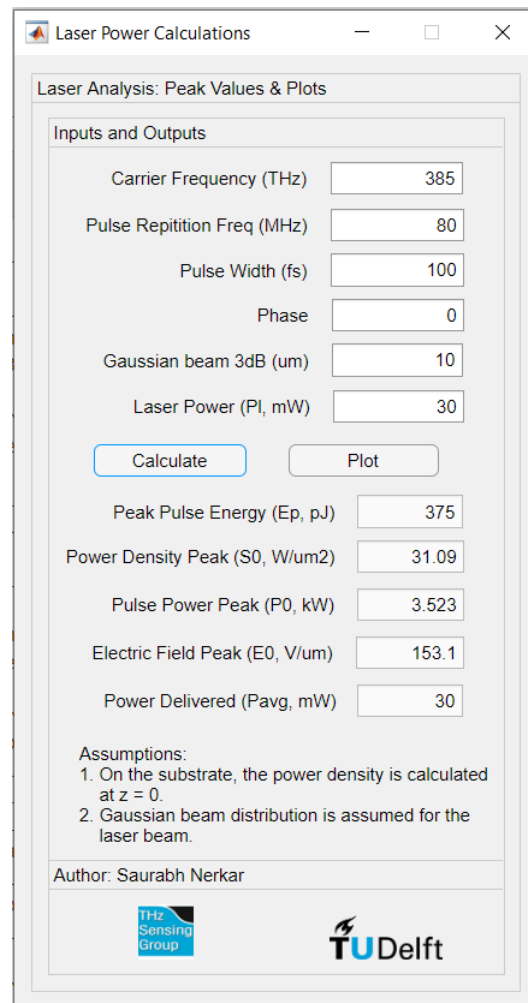


Figure A.1: Radar GUI: Tx Window: Laser Beam Analysis window

The inputs and output calculations can be summarized as below:

Table A.1: Nomenclature used in this document.

Input		Output	
Carrier Frequency	385 THz	Peak pulse energy	375 pJ
Pulse Repetition Frequency	80 MHz	Power Density Peak	31.09 W/ μm^2
Pulse Width	100 fs	Pulse Power Peak	3.523 kW
Phase	0	Electric Field Peak	153.1 V/ μm
Gaussian Beam -3 dB radius	10 μm		
Average Laser Power	30 mW		

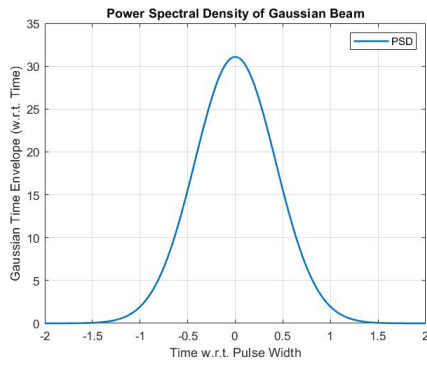


Figure A.2: Power spectral density of the laser beam

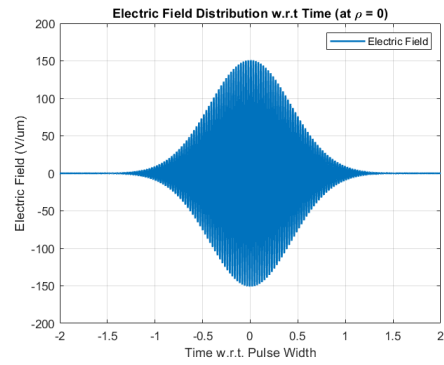


Figure A.3: Spatial distribution of electric field of laser

Appendix B

Time-Varying Conductance Of Photoconductor Source

Apply Ohm's law and assume the current impulse response to an applied electric field is instantaneous [20] [28], one comes to the relation expressed in Eq. (B.1) below:

$$\mathbf{j}(\mathbf{r};t) = \boldsymbol{\sigma}(\mathbf{r};t)\mathbf{e}(\mathbf{r};t) \quad (\text{B.1})$$

Current flowing through the gap in Fig. 2.2(a), if significant current is oriented across \hat{y} , is given as,

$$i(t) = \frac{1}{W_y} \int_{-W_y/2}^{W_y/2} \int_{-W_x/2}^{W_x/2} \int_{-W_z}^0 \mathbf{j}(\mathbf{r};t) \cdot \hat{\mathbf{y}} dz dx dy \quad (\text{B.2})$$

The voltage drop across the gap is,

$$v(t) = - \int_{-W_y/2}^{W_y/2} \mathbf{e}(\mathbf{r};t) \cdot \hat{\mathbf{y}} dy = e_y(0;t)W_y \quad (\text{B.3})$$

The current across the gap is approximately,

$$i(t) \approx g(t)v(t) \quad (\text{B.4})$$

Here, $g(t)$ is the time-dependant conductance of the photoconductor gap, it is given by below equation:

$$g(t) = \frac{1}{W_y^2} \int_{-W_y/2}^{W_y/2} \int_{-W_x/2}^{W_x/2} \int_{-W_z}^0 \boldsymbol{\sigma}(\mathbf{r};t) dz dx dy \quad (\text{B.5})$$

Above relation can also be expressed below [28]:

$$g(t) = \eta(W_x, W_y, W_z, A_{laser}) \frac{A_{laser}}{W_y^2} e\mu h(t) \otimes \tilde{s}(t) \quad (\text{B.6})$$

where, $h(t)$ is the impulse response of the material with respect to the laser excitation, it is given by Eq. (2.2), μ is the mobility of the charge carriers in the semiconductor gap which is obtained using the relation (B.8), e is the charge of an electron and \otimes define the time convolution following the relation mentioned below,

$$s(t) \otimes h(t) = \int_{-\infty}^{\infty} s(t - \tau)h(\tau)d\tau \quad (\text{B.7})$$

$$\mu = \frac{\text{mass of electron}(e)}{\text{relative mass of electron}(m_e)} * \text{scattering time}(\tau_s) \quad (\text{B.8})$$

The term η is known as the laser power absorption efficiency of the photoconductor gap. This property takes into account multiple factors viz., spillover of the laser beam with respect to the photoconductor gap size, the reflection at the air-photoconductor interface and the laser power absorption property of the photoconductor (characterized by α). η is given as below:

$$\eta(W_x, W_y, W_z, A_{laser}) = (1 - |\Gamma|^2) \frac{1 - e^{-\alpha W_z}}{W_z} \cdot \frac{1}{A_{laser}} \int_{-W_y/2}^{W_y/2} \int_{-W_x/2}^{W_x/2} \int_{-W_z}^0 |\tilde{s}_n(\boldsymbol{\rho}; z = 0) dz dx dy \quad (\text{B.9})$$

A_{laser} is the area of the spatial distribution with unitary amplitude of the laser beam Poynting vector at the photoconductor interface [20]. A_{laser} is defined in appendix A. Also, as previously seen, $h(t)$ is the impulse response of of the photoconductor material to laser excitation and $\tilde{s}(t)$ is the time varying envelope of the laser pulse.

Appendix C

List of Abbreviations

List of abbreviations

BW	Bandwidth
CW	Continuous Wave
EM	Electromagnetic
GUI	Graphical User Interface
FoV	Field of View
FPA	Focal Plane Array
FT	Fourier Transform
LWA	Leaky Wave Antenna
PCA	Photoconductive Antenna
PCCA	Photoconductive antenna Connected Array
PRF	Pulse Repetition Frequency
PRT	Pulse Repetition Time
PO	Physical-Optics
PW	Pulsed Wave
QO	Quasi-Optical
Rx	Receiver
SNR	Signal to Noise Ratio
THz	Terahertz
Tx	Transmitter

Appendix D

Nomenclature

Nomenclature used in the report is define as below.

Table D.1: Nomenclature used in this document.

Quantity	Notation
Scalar	a
Vector in space domain	\mathbf{a}
Unit vectors	$\hat{\mathbf{x}}$
Convolution	\otimes
Scalar or dot-product	\cdot
Width of a semiconductor gap (along x)	W_x
Length of a semiconductor gap (along y)	W_y
Height of a semiconductor gap (along z)	W_z
Power Spectral Density of the Lasers	S_{laser}
Bias Voltage of the PCA element	V_b or V_{bias}
Time-varying conductance across the semiconductor gap	$g(t)$
Impulse response of the semiconductor w.r.t. laser excitation	$h(t)$
Speed of light	c
Frequency	f
Area of laser beam	A_{laser}
Laser power absorption efficiency of photoconductor gap	$\eta(W_x, W_y, W_z, A_{laser})$ or η_{opt}
Mobility of charge carriers in photoconductor	μ
Recombination time of charge carriers in photoconductor	τ_c
Scattering time of charge carriers in photoconductor	τ_s
Plank's constant	h

Table D.2: Nomenclature used in this document.

Quantity	Notation
Band gap frequency of photoconductor	f_g
Charge of an electron	e or q_e
Current induced across photoconductor gap (time domain)	$i(t)$
Current induced across photoconductor gap (frequency domain)	$I_g(\omega)$
Fourier Transform of photoconductor impulse function	$H(\omega)$
Fourier Transform of power density function of laser	$S(\omega)$
Antenna Impedance of the antenna	$Z_a(\omega)$
Generator Impedance of the antenna	$Z_g(\omega)$
Pulse repetition time	T_p
Pulse repetition frequency	f_p
Pulse width of the wave	τ_p
Average Laser Power	\tilde{P}_{laser} or P_{laser} or P_l
Frequency of operation of laser	f_l
Constant resistance of the photoconductor gap	R_{gap}
Electric field across semiconductor gap	$e(\mathbf{r};t)$
Frequency of operation of laser	f_l
Energy spectrum of the PCA	E_s
Energy radiated by a PCA	E_{rad}
Power radiated by a PCA	P_{rad}
Energy available for radiation for the PCA	$E_{available}$
Power available for radiation for the PCA	$P_{available}$
Lateral resolution of the radar	δ_p
Range resolution of the radar	δ_r
Reflection efficiency of the target	η_{ref}
Efficiency of Tx and Rx	η_{Tx} and η_{Rx}
Number of pixels in 'p'	N_p
Diameter of reflector	D
f-Number of the reflector	N_f
Detection bandwidth of the radar	BW_n

Table D.3: Nomenclature used in this document.

Quantity	Notation
Acquisition time of the radar	T_{acq}
Integration time of the radar	T_{int}
QO Channel efficiency	η_{QO}
Energy received by each photoconductor gap	E_i^{Rx}
Power received by each photoconductor gap	P_i^{Rx}
Voltage induced in each photoconductor gap by a single pulse	$v_{\tau,i}$
Average voltage induced in single photoconductor gap	v_{avg}
Average noise voltage of the PCA gap	$\langle v_n \rangle$
Johnson noise level of the PCA gap	$\langle s_{v,n} \rangle$
Relative mass of electron	m_e
Reflection constant of the air-photoconductor gap interface	Γ
Conductivity of the photoconductor gap	$\sigma(\mathbf{r};t)$
Spatial distribution of the laser beam	$\tilde{s}_n(\boldsymbol{\rho};z=0)$
Characteristic impedance of the photoconductor gap	η_d

